dispersed in saline containing 0.05% Tween 80. These were commonly observed to be a mixture of well dispersed fine particles and agglomerates. $C_{60}$ was frequently agglomerated, but fine particles were also observed either individually or within pear-shaped agglomerates. In contrast, CB was relatively well dispersed, and agglomerates were occasionally present. In the case of kaolin, low-density tabular structures with rectangular or hexagonal shape were characteristically observed. The size distribution of materials used in the present study was analyzed by dynamic light scattering (DLS). $C_{60}$ demonstrated a wide distribution with ranges of 10.5 to 12913.9 nm, and most abundant sizes were two peaks at 234.1 ± 48.9 and 856.5 ± 119.2 nm, respectively. CB particles formed a normal distribution with ranges of 13.6 to 337.4 nm and major peak average was at around 232.0 nm. In the case of kaolin, a major peak average was 357.6 ± 199.4 nm belonging to a range of 5.1 to 4846.9 nm. Although the primary particle size of kaolin was 4.8 μm, it is likely that sonication might lead to size reduction.

### In vitro *micronucleus test*

To examine the genotoxicity of particles, we analyzed the micronucleus inducing activity of $C_{60}$, CB and kaolin using human lung cancer cell line, A549. A six-hour treatment of 200 μg/mL CB and kaolin caused growth inhibition of 60% in A549 cells; however, $C_{60}$ did not inhibit growth of cells at any concentrations (between 0.02 - 200 μg/mL, data not shown). As shown in Figure 2, $C_{60}$ and kaolin particles increased the number of micronucleated cells in a dose-dependent manner. On the other hand, CB increased the number of micronucleated cells up to 2 μg/mL, and thereafter seemed to plateau. The background frequency of micronucleated cells was 0.7% to 1.0%, and the frequency rose to 10% and 5% at 200 μg/mL of $C_{60}$ and kaolin, respectively, and 3.3% at 2 μg/mL of CB treatment. The increase of the frequency from that of the control cells was statistically significant in all particle-treated cells. $C_{60}$ demonstrated the most strong genotoxic/clastogenic potencies among these three particles.

### In vivo *genotoxicity analyzed by alkaline comet assay*

DNA damage induced by particles was evaluated using comet assay under alkaline conditions. Figure 3 shows the mean values of DNA tail moment in the lungs with or without single-particle treatment at 0.2 mg/body for 3 hr. In the case of particle exposure, DNA damage was significantly increased as compared with the vehicle control up to 2 - 3 fold, and its intensity was $C_{60}$ > CB > kaolin. On the other hand, we examined the genotoxicity of nano/microparticles at a dose of 0.05 mg/animal. DNA damage observed in the lung of mice was almost the same as those of the vehicle control (data not shown). Moreover, we examined the effects of different exposure times for 3 and 24 hr. While DNA damages induced by CB or kaolin were not changed either for 3 or 24 hr, DNA damage caused by $C_{60}$ was decreased for 24 hr compared with 3 hr (data not shown). It seems that DNA damage repair enzymes might affect the result of comet assay.

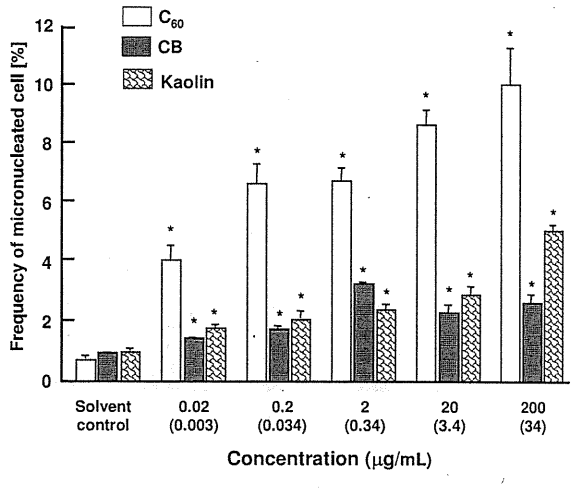


**Figure 2**
**Frequency of micronucleated A549 cells incubated with $C_{60}$ CB or kaolin.** The values represent the mean of three experiments ± SD. An asterisk (*) represents that each frequency is significantly different ($p < 0.01$) from that of control cell in a Student's t-test. Concentrations in μg/cm² are given in parenthesis.

### *General observations of* gpt *delta transgenic mice administrated with particles*

Body weights of *gpt* delta mice receiving a single dose of vehicle control reached 31.1 ± 1.8 g at 12 weeks after instillation. Values for *gpt* delta mice which received a single dose of particles at 0.2 mg/body were 30.0 ± 2.4 g for $C_{60}$, 32.6 ± 1.1 g for CB and 30.8 ± 2.3 g for kaolin, respectively, at 12 weeks after instillation. The average consumption of diet per day per mouse was 3.6 g, with no effects from particle instillation. No body weight and diet consumption changes were also observed with multiple doses of particles. All mice used for the single dose study survived to the end of the study, although, in the case of multiple doses, one fullerene- and one kaolin-administrated mouse died within two weeks after the last instillation, probably due to respiratory disturbances.

### gpt *Mutations in the lungs of* gpt *transgenic mice with particle treatment*

To determine the mutagenic effects of particles in the lungs, *gpt* delta transgenic mice were exposed to $C_{60}$, CB and kaolin at doses of 0.2 mg/body by single intratracheal instillation, and mutations were analyzed. Figure 3 shows the mutant frequencies (MFs) of the lungs. The back-

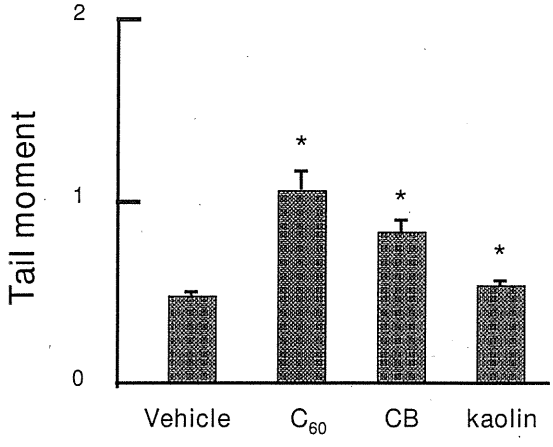


**Figure 3**
**DNA damage in lungs of C57BL/6J mice intratracheally instilled with particles.** DNA damage was measured by comet assay. Male mice were treated at a dose of 0.2 mg per animal of particles, and mice were sacrificed 3 hr after particle administrations. The values represent the mean of five animals ± SE. An asterisk (*) denotes $p < 0.01$ in a Dunnett's test after one-way ANOVA of Tail Moment of particle-treated vs. corresponding vehicle-control mice.

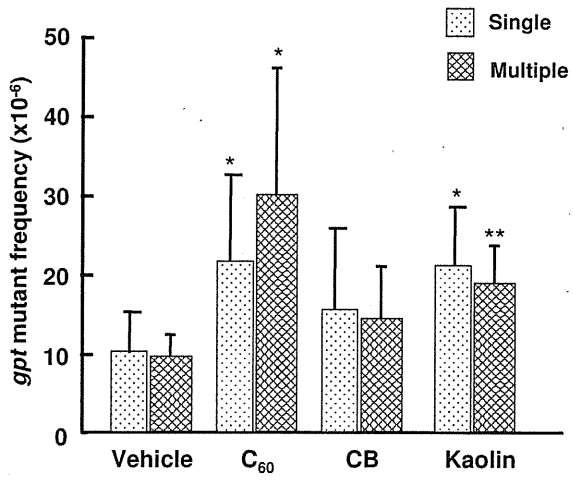


**Figure 4**
***gpt* MFs in the lungs of mice singly and multiply intratracheally instilled with particles.** Male mice were treated with single (0.2 mg per animal) or multiple (0.2 mg per animal × 4) doses of particles, and mice were sacrificed 12 (single) and 8 (multiple) weeks after particle administrations. Mean values ± SD are shown. An asterisk (*, **) denotes $p < 0.05$ (*) and $p < 0.01$ (**) in a Student's *t*-test of MF of particle-treated vs. the corresponding vehicle-control mice.

ground MF of lungs was 10.30 ± 0.53 × $10^{-6}$. MFs in the lungs induced by $C_{60}$ and kaolin were significantly increased by 2-fold compared with vehicle-instilled animals. CB showed increasing tendency for MF in the lungs, but not statistically significant.

Next, we examined the mutagenic effects of consecutive exposure of particles. The *gpt* MFs in the lungs obtained from mice multiply exposed (4 times) to 0.2 mg/body each of $C_{60}$, CB or kaolin are shown in Figure 4. In cases of $C_{60}$ and kaolin, MFs of the lungs were significantly higher as compared to those of control animals, and their values were 2 - 3 fold increased. In the case of CB exposure, MFs were slightly increased but not statistically significant.

To analyze the mutational characteristics induced by particles, we examined PCR and DNA sequencing analysis of 6-thioguanine (6-TG)-resistant mutants. More than 40 independent 6-TG resistant mutants derived from multiple particle instillation (0.2 mg × 4), and 25 mutants from vehicle instilled animals were identified. Classes of mutations found in the *gpt* gene are listed in Table 1. Base substitutions predominated with both particle-induced and spontaneous cases. No A:T to T:A and G:C to C:G transversions were detected in vehicle control groups, indicating that these types of mutations are rare events in the spontaneous mutations. Interestingly, G:C to C:G transversion commonly increased in all three particle treatments compared to the vehicle control. G:C to A:T transition also significantly increased in CB and kaolin instillation but not in $C_{60}$. In addition, the numbers of A:T to T:A transversion were slightly increased in the treatment with $C_{60}$ and CB. Other types of mutations, including deletions and insertions, were also observed in both particle-treated and vehicle control groups, but these were of minor significance.

The distribution of spontaneous and particle-induced mutations in the *gpt* gene is shown in Figure 5. Base substitutions were spread throughout the coding region with a preference for some sites. However, clear mutational hotspots for each particle could not be seen except deletion mutations occurring at a run of 5 adenines (positions 8 to 12) and at position 244 for $C_{60}$ treatment. The distribution of base substitutions along the *gpt* gene did not vary with the particle types. Twelve out of 200 particle-induced mutations occurred at position 64, eighteen at position 110, ten at position 115. All of the base substitutions occurring at positions 110 and 115 were G to A transitions, and at position 64 were C to T transitions, which were common among spontaneous mutants. In contrast, four to eight mutations occurred at positions 116, 143,

**Table 1: Classification of *gpt* mutations from the lungs of control and particle multiply (0.2 mg × 4) treated mice[a)]**

| | Control | | $C_{60}$ | | CB | | Kaolin | |
|---|---|---|---|---|---|---|---|---|
| Type of mutation in gpt | No. | % | No. | % | No. | % | No. | % |
| Base substitutions | | | | | | | | |
| Transitions | 10 | 40 | 35 | 41 | 18 | 45 | 37 | 50 |
| A:T->G:C | 2 | 8 | 11 | 13 | 2 | 5 | 5 | 7 |
| G:C->A:T | 8 | 32 | 24 | 28 | 16 | 40 | 32 | 43 |
| Transversions | 10 | 40 | 35 | 40 | 17 | 43 | 30 | 41 |
| A:T->T:A | 0 | 0 | 2 | 2 | 1 | 3 | 0 | 0 |
| A:T->C:G | 2 | 8 | 3 | 3 | 4 | 10 | 5 | 7 |
| G:C->T:A | 8 | 32 | 25 | 29 | 8 | 20 | 17 | 23 |
| G:C->C:G | 0 | 0 | 5 | 6 | 4 | 10 | 8 | 11 |
| Deletions | 4 | 16 | 12 | 14 | 4 | 10 | 6 | 8 |
| Insertions | 1 | 4 | 3 | 4 | 0 | 0 | 1 | 1 |
| Others | 0 | 0 | 1[b)] | 1 | 1[C)] | 3 | 0 | 0 |
| Total | 25 | 100 | 86 | 100 | 40 | 101 | 74 | 100 |

[a)]Independent mutations were isolated no more than once from any individual mouse.
[b)]Multiple mutation (Four base substitutions)
[C)]Tandem mutation (GG->TT)

189, 320, 406 and 418 were only seen in the particle-treated mice, therefore it is suggested that these mutations can be considered as particle-induced mutations. Among these, five out of six mutations at position 406 were found in $C_{60}$ instillation, and all mutation patterns were G to T transversions. Four out of 7 and five out of 8 at positions 189 and 418 were detected in kaolin instillation, and the majorities of the mutations were G to A and C to A, respectively. Moreover, these hotspots induced by particles occurred at G or C residues in the *gpt* gene without association for specific sequences.

### *Spi⁻ MFs in the lungs of gpt transgenic mice with particle treatment*

We also measured the Spi⁻ MFs in the lungs of *gpt* delta mice instilled with multiple doses (0.2 mg × 4) of particles (Figure 6). Spi⁻ MFs of the vehicle control was 4.85 ± 2.04 × $10^{-6}$, in contrast, particle-administrated groups were 4.91 ± 3.03 × $10^{-6}$ for $C_{60}$, 6.87 ± 4.06 × $10^{-6}$ for CB and 8.12 ± 3.32 × $10^{-6}$ for kaolin. As shown in Figure 6, Spi⁻ MFs in the lungs of the CB- and kaolin-treated, but not $C_{60}$-treated groups were increased, and in particular, the values of the kaolin-treated groups were significantly elevated up to 2-fold.

### *gpt Mutations in the kidneys of gpt transgenic mice with particle treatment*

To determine the tissue distribution and specificity of particles with intratracheal instillation, *gpt* MFs of the kidney were analyzed. *gpt* MFs of the vehicle control versus particle-multiple administrated groups (0.2 mg × 4) were 1.33 ± 0.51 × $10^{-5}$ versus 1.67 ± 0.66 × $10^{-5}$ for $C_{60}$, 1.03 ± 0.39 × $10^{-5}$ for CB and 1.32 ± 0.32 × $10^{-5}$ for kaolin. From these observations, it is suggested that these particles did not induce mutation in the kidneys under these conditions.

### *Histopathological evaluation*

Histopathological analyses of lung tissues of *gpt* delta mice consecutively instilled particles, $C_{60}$, CB and kaolin, at 0.2 mg/body per week for 4 weeks each are shown in Figure 7. Test substances-phagocytized alveolar macrophages were diffusely found in the lungs, but not in the vehicle group. Focal granulomatous formation accompanied with or without the test substance-phagocytized macrophages were also frequently observed in the lungs of particle-multiply-instilled mice. Similar findings, but a slight degree of particle accumulation and granuloma formation, were also observed in lungs of mice with particle single-instillations (data not shown). The degree of granuloma formation in the lungs of multiple $C_{60}$- or CB-exposed mice appeared more severe than those in multiple kaolin-exposed mice. No abnormalities were observed in the kidneys obtained from mice multiply instilled with particles (data not shown).

## Discussion and conclusion

This study demonstrated the genotoxicity of nano/micro-particles widely used for industrial, cosmetic and medical fields. In *in vitro* genotoxic analysis, increased MN frequencies were observed in A549 cells treated with $C_{60}$, CB and kaolin in a dose-dependent manner. On the other hand, these three particles also induced DNA damage in the lungs of C57BL/6J mice measured by comet assay. Furthermore, we found that $C_{60}$ and kaolin demonstrated mutagenicity either or both of *gpt* and Spi⁻ mutations in the *gpt* delta transgenic mice systems. The *gpt* gene MFs were significantly increased in the lungs of *gpt* delta mice with $C_{60}$ and kaolin, but not CB administrations. A dose-dependent MF increase was observed in the lungs of $C_{60}$, but not kaolin treated groups. The reason is still unclear, but suggesting that the single dose of kaolin already repre-

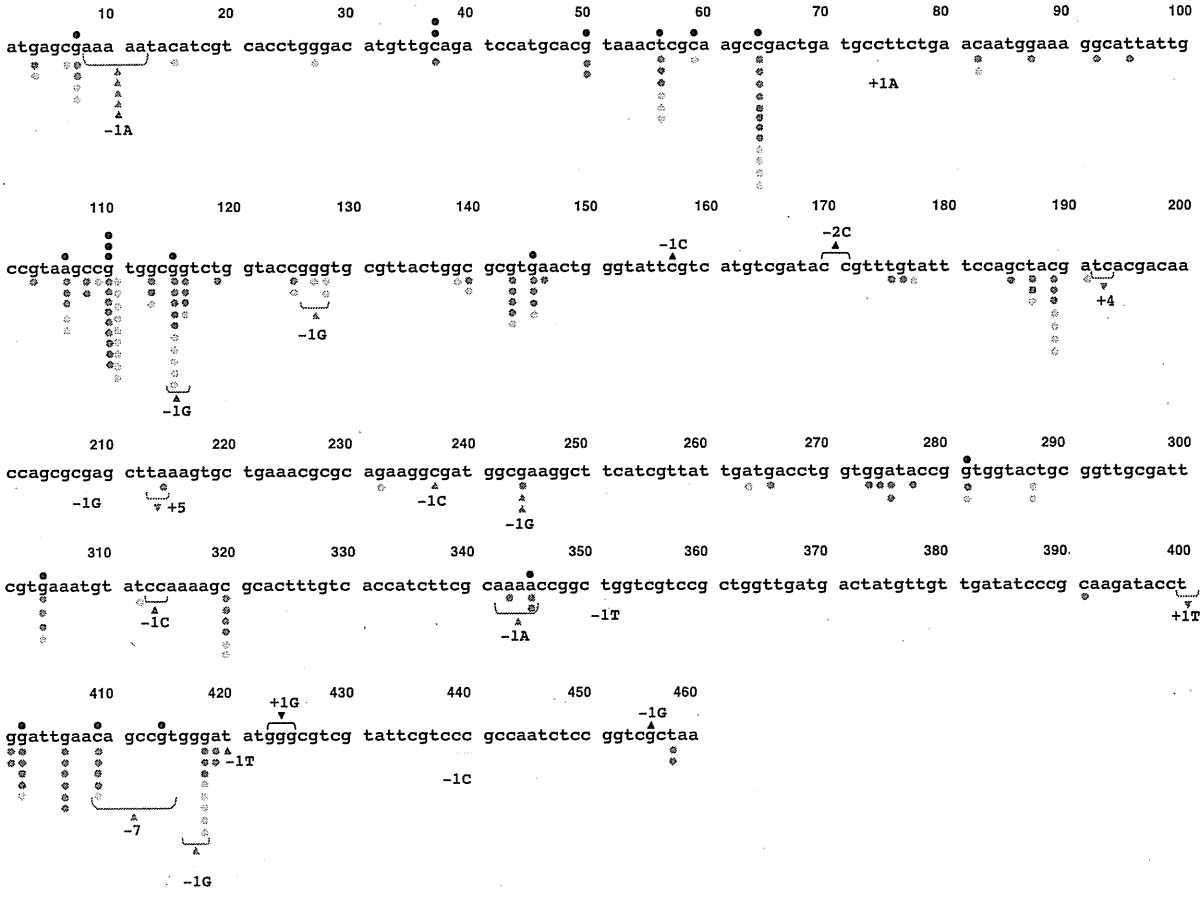


**Figure 5**

**Spontaneous and particle-induced mutations in the coding region of the *gpt* gene.** Mutations obtained from the control mice are shown above the wild type sequence, and mutations obtained from the particle-treated mutant clone are shown below the wild type sequence. The types of particles are indicated by color coding: red for $C_{60}$, blue for CB and sky blue for kaolin. Mutation types, base substitution, and deletion and insertion are indicated by circle, triangle, and inverted triangle, respectively.

sented the maximum response. On the other hand, kaolin demonstrated significantly increased Spi- MFs; however, $C_{60}$ showed similar values compared with the vehicle control of the lungs. Spi- selection detects deletions in size more than 1 bp and 10 kb [24]; therefore, additional DNA damages involved in deletion mutations might be induced by kaolin. It, it is also suggested that $C_{60}$ does not prefer to induce such kinds of DNA damages under these conditions. In contrast to the present study, Xu *et al.* have reported that $C_{60}$ dramatically increases large deletion mutations in *gpt* delta transgenic mouse primary embryo fibroblast cells [25]. The observed difference of mutational signatures of $C_{60}$ between a cell line and lung tissue might be related to differences between *in vitro* and *in vivo* assay systems in DNA damage formations, DNA repair or translesion DNA synthesis.

To further elucidate the mechanisms behind the increase in mutant frequency observed in this study, we analyzed mutation spectra using a PCR-direct sequencing method. Most mutations induced by three particles in the present study, occurred at G:C base pairs (52/76, 68%). Among these, 13 G:C base pairs were located in the G or C runs. The most prominent hot spots were at base pairs 143, 189, 320, 406 and 418, and there were no significant differences in the distributions of mutation hot spots in the three particles. This may reflect the distribution of DNA damage sites caused by particles. The most prominent mutation type induced by particles was G:C to C:G transversion. Since these mutations were commonly increased regardless of the constituents of particles (i.e. $C_{60}$ and CB were graphite and kaolin was aluminum silicate), it is suggested that mechanisms leading to the induction of such

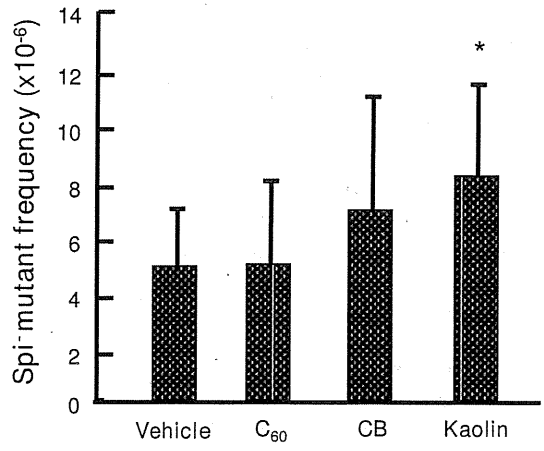


**Figure 6**
**MFs of deletions in the lungs of *gpt* delta mice exposed to multiple doses of particles.** An asterisk (*) denotes $p < 0.05$ in a Student's *t*-test of MFs of particle-treated vs. the corresponding vehicle-control mice.

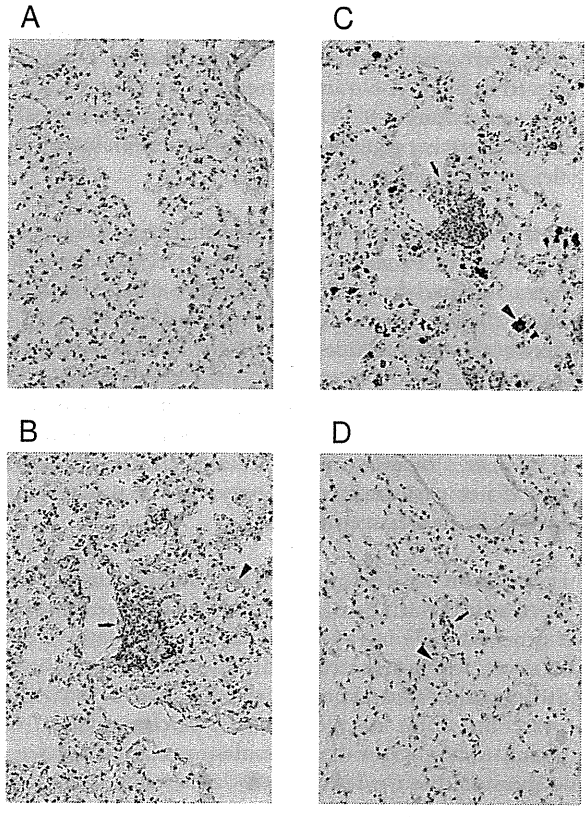


**Figure 7**
**Microscopic findings in lungs of *gpt* delta mice intratracheally instilled with particles.** Normal appearance of pulmonary parenchyma in a vehicle-control (Panel A). Pulmonary parenchyma obtained from *gpt* delta mice intratracheally instilled with four consecutive doses of 0.2 mg/mice of $C_{60}$ (Panel B), CB (Panel C) and kaolin (Panel D). Test substance-phagocytized macrophages (arrowheads) can be observed, and granulomaous (arrows) formations are also found in lungs of particle-instilled mice. A-D; Original magnification × 40.

kinds of mutations might be same. In general, the G:C to C:G transversion is thought to be a rare event in both spontaneous and chemically-induced mutations. However, various oxidative stresses caused by sunlight, UV radiation, hydrogen peroxide and peroxy radicals frequently induce G:C to C:G transversion in *in vitro* assay systems [26-29]. Reactive oxygen species (ROS) and DNA damage, including 8-oxo-7,8-dihydro-2'-deoxyguanosine (8-oxo-dG), were reported to be increased by nanoparticles, including asbestos, treatment [4,21,30-34]. The mechanism of the generation of ROS by nanoparticles is still unclear; however, these nanoparticles would be able to trigger ROS production by iron-catalysed Fenton reactions, or would be accumulated in the cells by phagocytosis, then enhance the production of ROS from macrophages and leucocytes [35,36]. In the present study, test substance-phagocytized macrophages and granulomas were frequently observed in the lungs, and the degree of the granulomas formation was partly associated with the mutagenic effect on *gpt* gene by particles. In the case of $C_{60}$, generation of ROS along with lipid peroxidation via electron transfer between $C_{60}$ and other molecules has been reported [21]. The most typical lesion of oxidative damage is 8-oxo-dG which can pair with dA and leads G to T transversions [37,38] but it is not responsible for G to C transversion since dG is not incorporated opposite 8-oxodG [37,39]. Moreover, a variety of oxidative lesion products of guanine other than 8-oxodG, including imidazolone (Iz), oxazolone (Oz), spiroiminodihydantoin (Sp) and guanidinohydantoin (Gh), have been reported [39-45]. Recently, three such molecules, Oz, Sp and Gh are thought to be the key molecules causing G to C transversion using the translesion synthesis systems [43-46]. Moreover, these molecules have also been detected in bacterial cells and rat liver [47,48]. Therefore, it is suggested that G:C to C:G transversions induced by particles such as $C_{60}$, CB and kaolin could involve Oz, Sp and Gh formations.

In the present study, G:C to A:T transition and A:T to T:A transversion were also increased in the particle treatment. G to A transition has commonly been observed in spontaneous and chemically-induced mutants and deamination of 5-methylcytosine or alkylation of guanine might be

involved in these mutations. In contrast to G to A transition, A:T to T:A transversion is known as a rare mutation. It has been reported that the most common mutations induced by N-ethyl-N-nitrosourea in the mouse are A:T to T:A transversions [49]. However, at present, the mechanisms underlying generation of A to T transversion by particles are still unclear.

As mentioned above, we found that all three particles, $C_{60}$, CB and kaolin increased significant DNA damage in the lungs compared to the vehicle control using the comet assay. Comet assay under alkaline conditions is used to detect both strand breaks and DNA altering lesions such as an AP site [50]. Moreover, in the present study, treatments with $C_{60}$, CB and kaolin significantly increased the frequency of micronucleated A549 cells in a dose-dependent manner. However, these genotoxic/clastogenic potencies did not necessarily correspond to the mutagenicity observed in *gpt* transgenic mice.

In conclusion, we demonstrated that manufactured nano/microparticles such as $C_{60}$, CB and kaolin were shown to be genotoxic in both *in vitro* and *in vivo* assay systems. Moreover, it was not necessarily the case that genotoxic potency was related to particle size ($C_{60}$ and CB are nano-sized, but kaolin is micro-sized particles used in the present study.). From the prominent mutation spectra, it is suggested that oxidative DNA damage might be commonly involved in their mutagenicity. The dose of particles used in the present study seems to be extremely high compared with human exposure in the work place. However, it is likely that these materials would be deposited for a long time in tissues, same as those of asbestos fiber. Therefore, further studies of the mechanisms of genotoxicity and application routes other than trachea are needed. Moreover, exposure levels of these genotoxic particles in the working environment should be determined.

## Materials and methods

### *Materials and chemicals*

CB nanoparticles with a primary particle size of 14 nm (Printex 90) were obtained from Degussa, Dusseldorf, Germany. The surface area was 300 $m^2/g$ (disclosed by Degussa). The CB was autoclaved at 250°C for 2 h before use. High purity (99.9%) $C_{60}$ was purchased from Sigma-Aldrich. (St. Louis, MO, USA). The declared primary particle size of $C_{60}$ was 0.7 nm. Kaolin, white crystal, with a primary particle size of 4.8 μm was obtained from Engelhard Corp., Iselin, NJ. $C_{60}$, CB and kaolin particles were suspended in saline (Otsuka Pharmaceutical Co. Ltd., Tokyo, Japan) containing 0.05% of Tween 80 (Nacalai Tesque, Kyoto, Japan) by sonication for 15 - 20 min, at a concentration of 2 mg/mL. The size distributions of the presently used nano/microparticles in the suspensions were measured by dynamic light scattering (DLS) using FPAR-1000 (Otsuka electronics Co., Ltd., Osaka), and the agglomeration state was assessed by transmission electron microscope (TEM) (H-7000, Hitach, Ltd., Tokyo, Japan). The size distributions were determined with the algorithm CONTIN. For the TEM assessment, an aliquot of 5 μL was put on the nickel glid coated by hydrophilized formbar and assessed with an accelerating voltage of 75 kV.

Type I agarose, low melting point agarose, dimethylsulfoxide and Triton X-100 were bought from Sigma-Aldrich. Ethidium bromide was obtained from Merck (Darmstadt, Germany). Other chemicals were purchased from Wako Pure Chemical Industries (Osaka, Japan).

### *Micronucleus test*

Human lung carcinoma A549 cells obtained from the RIKEN Cell Bank (Wako, Japan) were cultured in Eagle's minimum essential medium (Nissui Pharmaceutical Co. Ltd., Tokyo, Japan) supplemented with 10% fetal bovine serum (JRH Biosciences, Lenexa, KS, USA) in a 5% $CO_2$ atmosphere at 37°C. The cells ($7 \times 10^5$ cells/dish) were seeded in plastic cell culture dishes (ϕ60 mm) one day before treatment. Particles were suspended in physiological saline containing 0.05% (v/v) Tween-80 with sonication (for 5-10 min at room temperature). One volume of the suspension was mixed with 9 volumes of the culture medium with serum (altogether 3.3 mL/dish), and then cells were treated at indicated concentrations for 6 hr. Since a long exposure (48 hr) increased the frequency of micronucleated cells in the solvent control (data not shown), we chose a 6 hr treatment. After treatment, cells were further cultured for 42 hr. Then, cells were trypsinized and counted, and centrifuged. Growth inhibition was calculated by following the formula:

Growth rate = (the number of treated cells) / (the number of non-treated cells)

Cells were resuspended in 0.075 M KCl, and incubated for 5 min. Cells were then fixed 4 times in methanol:glacial acetic acid (3:1), and washed with methanol containing 1% acetic acid. Finally, cells were resuspended in methanol containing 1% acetic acid. The cell solution was dropped onto slides and the nucleus was stained by mounting with 40 μg/mL acridine orange (Nacalai Tesque) solution and immediately observed by fluorescence microscopy using blue excitation. The number of cells with micronuclei was recorded based on observation of 1,000 interphase cells. The data of EMS and mitomycine C (MMC) for positive system controls in CHL cells under the same experimental conditions were as follows; Percentage of micronucleated cells were 9.8 ± 0.68 for EMS (1 mg/mL) and 10.3 ± 1.1 for MMC (100 n/mL), respectively.

### *Animals*

Male C57BL/6J mice (9 weeks old) were purchased from Charles River Japan, Inc. (Atsugi, Japan) and *gpt* delta mice (9 weeks old) were obtained from Japan SLC (Shi-

zuoka, Japan), respectively. The *gpt* delta mice carry approximately 80 copies of *lambda* EG10 DNA on each chromosome 17 on a C57BL/6J background [23]. Animals were provided with food (CE-2 pellet diet, CLEA Japan, Inc., Tokyo, Japan) and tap water *ad libitum* and quarantined for one week. Mice were maintained under controlled conditions: 12-h light/dark cycle, 22 ± 2°C room temperature, and 55 ± 10% relative humidity. The experiments were conducted according to the "Guidelines for Animal Experiments in the National Cancer Center" of the Committee for Ethics of Animal Experimentation of the National Cancer Center.

### *Treatment of wild type and gpt delta transgenic mice with particles*

All particles were well sonicated and suspended in saline containing 0.05% of Tween 80. For comet assay, 5 male C57BL/6J mice were intratracheally instilled with particles using a polyethylene tube under anesthesia with 4% halothane (Takeda Chemical, Osaka, Japan). Single doses of 0.05 or 0.2 mg per animal were employed. The control mice (n = 5) were instilled intratracheally with 0.1 mL of the solvent alone. The mice were sacrificed 3 hr after these particle administrations, and lungs were removed then used for comet assay immediately. In addition, different exposure time (24 hr) was also examined. For histological and mutation analysis, each group of 10 male *gpt* delta mice was intratracheally instilled with particles at a single dose of 0.2 mg per animal, and multiple doses of 0.2 mg per animal per week for 4 consecutive instillations, as described for comet assay. The intratracheal instillation dose of particles between 0.05 and 1 mg/mouse has been commonly used for the pulmonary inflammation and genotoxicity test [51,52]. The control mice (n = 10) were instilled intratracheally with the solvent alone. The mice were sacrificed at 22 weeks old being 12 (for single instillation) or 8 (for multiple instillations) weeks after particle administrations, respectively. Tissues, including lungs and kidneys, were removed. Lungs and kidneys obtained from 4 mice were used for histological evaluation and examined under a light microscope for any abnormalities. For histopathological evaluation, organs were fixed in 10% neutral buffered formalin, embedded in paraffin blocks and routinely processed to H&E stained sections. The remaining 6 mice were used for mutation analysis and the tissues were stored at -80°C until the DNA was isolated.

### *Alkaline comet assay*

The alkaline comet assay was performed according to the method of Sasaki et al. [53] or Toyoizumi et al. [54] with some modification. The lungs were taken from treated mice and weighed, and lung tissue was minced and suspended with chilled homogenizing buffer, then homogenized gently using a Dounce-type homogenizer in ice. Lung cell suspension was mixed with the same volume of 1.4% low melting point agarose in PBS. The mixture was layered on the slide coated with 0.7% agarose layer, and then covered with 0.7% low melting point agarose. After slide preparation, slides were immersed in lysing solution and refrigerated at 4°C for 1 h. Each slide was then placed in alkaline electrophoresis buffer for 10 min to allow for DNA unwinding. Electrophoresis was performed at 25 V, 300 mA for 15 min at 0°C. The slides were neutralized with Tris buffer for 5 min twice, and dehydrated with 70% ethanol to fix. The cells were stained with ethidium bromide solution. Comet images were analyzed using a fluorescence microscope (magnification 200×) equipped with a CCD camera. Fifty cells were examined per mouse. The tail moment of DNA was measured using Comet Analyzer Youworks Bio Imaging Software.

### gpt *and Spi⁻ mutation assays*

High-molecular-weight genomic DNA was extracted from the lungs and kidneys using a RecoverEase DNA Isolation Kit (Stratagene, La Jolla, CA) according to the instruction manual provided by the supplier. *Lambda* EG10 phages were rescued using Transpack Packaging Extract (Stratagene).

The *gpt* mutagenesis assay was performed according to previously described methods [55]. Briefly, *E. coli* YG6020 was infected with the phage and spread on M9 salt plates containing Cm and 6-TG, then incubated for 72 hr at 37°C. This enabled selection of colonies harboring a plasmid carrying the gene for chloramphenicol acetyltransferase, as well as a mutated *gpt*. Isolate exhibiting the 6-TG-resistant phenotype was cultured overnight at 37°C in LB broth containing 25 mg/mL Cm, then harvested by centrifugation (7,000 rpm, 10 min), and stored at -80°C.

The mutation spectrum of 6-TG cording sequence were performed by PCR and direct sequencing. Briefly, a 739 bp DNA fragment containing *gpt* was amplified by PCR as described previously [30,53]. Sequencing analysis was done at Takara Bio Inc. (Mie, Japan).

The Spi⁻ assay was performed as described previously [53]. The lysates of Spi⁻ mutants were obtained by infection of *E. coli* LE392 with the recovered Spi⁻ mutants. *gpt* and Spi⁻ MFs were determined in each mouse and the means ± standard deviations were calculated.

### *Statistical analysis*

The data from micronucleus test and *gpt* and Spi⁻ mutation assay are expressed as mean ± standard deviations. The data obtained from comet assay are expressed as mean ± standard errors. The data were statistically compared with the corresponding solvent control using the Student's t-

test for micronucleus and *gpt* and Spi- mutation assay. To test for significant differences of tail moment in the comet assay between a group treated with materials and an untreated group, Dunnett's test after one-way ANOVA was used to evaluate the differences; *p* values lower than 0.05 were considered to indicate statistical significance.

## Abbreviations

CB: carbon black; $C_{60}$: fullerenes; MN: micronuclei; CNTs: carbon nanotubes; TEM: transmission electron microscope; DLS: dynamic light scattering; MFs: mutant frequencies; 6-TG: 6-thioguanine; 8-oxo-dG: 8-oxo-7,8-dihydro-2'-deoxyguanosin; Iz: imidazolone; Oz: oxazolone; Sp: spiroiminodihydantoin; Gh: guanidinohydantoin; ROS: reactive oxygen species.

## Competing interests

The authors declare that they have no competing interests.

## Authors' contributions

YT carried out the preparation and performance of *gpt* delta transgenic mouse experiments and drafted the manuscript. SO and MK performed *in vitro* MN tests. TK and SM performed the comet assay. TI, KH and TH performed the animal exposure and *gpt* and Spi- mutation analysis. Pulmonary and renal histopathological evaluations were done by TI and AN. Analysis of size distribution and agglomeration state of particles were done by MW and NF. TN, NK, TY, TS and KW conceived and supervised the study. All authors read and approved the final manuscript.

## Acknowledgements

We thank Mr. Naoaki Uchiya, Ms Hiroko Suzuki, Yoko Matsumoto, Naoki Itcho and Mitsuyo Fujii for excellent technical assistance. This study was supported by Grants-in-Aid for Cancer Research and for Research on Risk of Chemical Substances from the Ministry of Health, Labour, and Welfare of Japan. Takashi Higuchi one of authors, is an awardee of a Research Fellowship from the Japan Food Hygiene Association for Promoted Project of Research on Risk of Chemical Substances from the Ministry of Health, Labour, and Welfare of Japan.

## References

1. Mazzola L: **Commercializing nanotechnology.** *Nat Biotechnol* 2003, **21**:1137-1143.
2. Paull R, Wolfe J, Hebert P, Sinkula M: **Investing in nanotechnology.** *Nat Biotechnol* 2003, **21**:1144-1147.
3. Elmore AR, Cosmetic Ingredient Review Expert Panel: **Final report on the safety assessment of aluminum silicate, calcium silicate, magnesium aluminum silicate, magnesium silicate, magnesium trisilicate, sodium magnesium silicate, zirconium silicate, attapulgite, bentonite, Fuller's earth, hectorite, kaolin, lithium magnesium silicate, lithium magnesium sodium silicate, montmorillonite, pyrophyllite, and zeolite.** *Int J Toxicol* 2003, **22(Suppl 1)**:37-102.
4. IARC: **Carbon Black and Some Nitro Compounds.** *IARC Monogr Eval Carcinog Risks Hum* 1996, **65**:149-262.
5. Hoet P, Bruske-Hohlfeld I, Salata O: **Possible health impact of nanomaterials.** In *Nanomaterials - Toxicity, health and environmental issues* Edited by: Kumar C. Weinheim: WILEY-VGH Verlag GmbH & Co. KGaA; 2006:53-80.
6. Bosi S, Da Ros T, Spalluto G, Prato M: **Fullerene derivatives: an attractive tool for biological applications.** *Eur J Med Chem* 2003, **38**:913-23.
7. IARC: **Diesel and gasoline engine exhausts and some nitroarenes.** *IARC Monogr Eval Carcinog Risks Hum* 1989, **46**:1-458.
8. Hesterberg TW, Bunn WB 3rd, Chase GR, Valberg PA, Slavin TJ, Lapin CA, Hart GA: **A critical assessment of studies on the carcinogenic potential of diesel exhaust.** *Crit Rev Toxicol* 2006, **36**:727-776.
9. Jacobsen NR, Møller P, Cohn CA, Loft S, Vogel U, Wallin H: **Diesel exhaust particles are mutagenic in FE1-MutaMouse lung epithelial cells.** *Mutat Res* 2008, **641**:54-57.
10. Hashimoto AH, Amanuma K, Hiyoshi K, Sugawara Y, Goto S, Yanagisawa R, Takano H, Masumura K, Nohmi T, Aoki Y: **Mutations in the lungs of *gpt* delta transgenic mice following inhalation of diesel exhaust.** *Environ Mol Mutagen* 2007, **48**:682-693.
11. Barrett JC, Lamb PW, Wiseman RW: **Multiple mechanisms for the carcinogenic effects of asbestos and other mineral fibers.** *Environ Health Perspect* 1989, **81**:81-89.
12. IARC: **Asbestos.** *IARC Monogr Eval Carcinog Risks Hum* 1997, **14**:11-106.
13. IARC: **Overall Evaluation of Carcinogenicity: An Updating of IARC Monographs.** *IARC Monogr Eval Carcinog Risks Hum* 1987, **1-42(suppl 7)**:106-117.
14. Baan RA: **Carcinogenic hazards from inhaled carbon black, titanium dioxide, and talc not containing asbestos or asbestiform fibers: recent evaluations by an IARC Monographs Working Group.** *Inhal Toxicol* 2007, **19(Suppl 1)**:213-228.
15. IARC: **Man-made Vitreouis Fibres.** *IARC Monogr Eval Carcinog Risks Hum* 2002, **81**:33-374.
16. Bunn WB 3rd, Bender JR, Hesterberg TW, Chase GR, Konzen JL: **Recent studies of man-made vitreous fibers. Chronic animal inhalation studies.** *J Occup Med* 1993, **35**:101-113.
17. Lam C-W, James JT, McCluskey R, Holian A, Hunter RL: **Toxicity of carbon nanotubes and its implications for occupational and environmental health.** In *Nanomaterials - Toxicity, health and environmental issues* Edited by: Kumar C. Weinheim: WILEY-VGH Verlag GmbH & Co. KGaA; 2006:130-152.
18. Donaldson K, Aitken R, Tran L, Stone V, Duffin R, Forrest G, Alexander A: **Carbon nanotubes: a review of their properties in relation to pulmonary toxicology and workplace safety.** *Toxicol Sci* 2006, **92**:5-22.
19. Poland CA, Duffin R, Kinloch I, Maynard A, Wallace WA, Seaton A, Stone V, Brown S, Macnee W, Donaldson K: **Carbon nanotubes introduced into the abdominal cavity of mice show asbestos-like pathogenicity in a pilot study.** *Nat Nanotechnol* 2008, **3**:423-428.
20. Takagi A, Hirose A, Nishimura T, Fukumori N, Ogata A, Ohashi N, Kitajima S, Kanno J: **Induction of mesothelioma in p53+/- mouse by intraperitoneal application of multi-wall carbon nanotube.** *J Toxicol Sci* 2008, **33**:105-116.
21. Nielsen GD, Roursgaard M, Jensen KA, Poulsen SS, Larsen ST: **In vivo biology and toxicology of fullerenes and their derivatives.** *Basic Clin Pharmacol Toxicol* 2008, **103**:197-208.
22. Jensen AW, Wilson SR, Schuster DI: **Biological applications of fullerenes.** *Bioorg Med Chem* 1996, **4**:767-779.
23. Nohmi T, Masumura K: **Molecular nature of intrachromosomal deletions and base substitutions induced by environmental mutagens.** *Environ Mol Mutagen* 2005, **45**:150-161.
24. Nohmi T, Suzuki M, Masumura K, Yamada M, Matsui K, Ueda O, Suzuki H, Katoh M, Ikeda H, Sofuni T: **Spi(-) selection: An efficient method to detect gamma-ray-induced deletions in transgenic mice.** *Environ Mol Mutagen* 1999, **34**:9-15.
25. Xu A, Chai Y, Hei T: **Genotoxic responses to titanium dioxide nanoparticles and fullerene in *gpt* delta transgenic MEFcells.** *Particle Fibre Toxicol* 2009, **6**:3.
26. Negishi K, Hao W: **Spectrum of mutations in single-stranded DNA phage M13mp2 exposed to sunlight: predominance of G-to-C transversion.** *Carcinogenesis* 1992, **9**:1615-1618.
27. Akasaka S, Yamamoto K: **Hydrogen peroxide induces G:C to T:A and G:C to C:G transversions in the supF gene of Escherichia coli.** *Mol Gen Genet* 1994, **243**:500-505.
28. Valentine MR, Rodriguez H, Termini J: **Mutagenesis by peroxy radical is dominated by transversions at deoxyguanosine: evidence for the lack of involvement of 8-oxo-dG1 and/or abasic site formation.** *Biochemistry* 1998, **37**:7030-7038.

29. Shin CY, Ponomareva ON, Connolly L, Turker MS: **A mouse kidney cell line with a G:C --> C:G transversion mutator phenotype.** *Mutat Res* 2002, **503**:69-76.
30. Jacobsen NR, Pojana G, White P, Møller P, Cohn CA, Korsholm KS, Vogel U, Marcomini A, Loft S, Wallin H: **Genotoxicity, cytotoxicity, and reactive oxygen species induced by single-walled carbon nanotubes andC(60) fullerenes in the FE1-Muta™ Mouse lung epithelial cells.** *Environ Mol Mutagen* 2008, **49**:476-487.
31. Valberg PA, Long CM, Sax SN: **Integrating studies on carcinogenic risk of carbon black: epidemiology, animal exposures, and mechanism of action.** *J Occup Environ Med* 2006, **48**:1291-1307.
32. Sayes CM, Marchione AA, Reed KL, Warheit DB: **Comparative pulmonary toxicity assessments of C60 water suspensions in rats: few differences in fullerene toxicity in vivo in contrast to in vitro profiles.** *Nano Lett* 2007, **7**:2399-2406.
33. Gao N, Keane MJ, Ong T, Wallace WE: **Effects of simulated pulmonary surfactant on the cytotoxicity and DNA-damaging activity of respirable quartz and kaolin.** *J Toxicol Environ Health A* 2000, **60**:153-167.
34. Kasai H, Nishimura S: **DNA damage induced by asbestos in the presence of hydrogen peroxide.** *Gann* 1984, **75**:841-844.
35. Aust A: **The role of iron in asbestos induced cancer.** In *Cellular and Molecular Effects of Mineral and Syntheticn Dusts and Fibers, NATO ASI Series Volume H85*. Edited by: Davis JMG, Jaurand M-C. Berlin: Springer-Verlag; 1994:53-61.
36. Mossman BT, Gee BL: **Pulmonary reactions and mechanisms of toxicity of inhaled fibers.** In *Toxicology of the Lung* 2nd edition. Edited by: Gardner, et al. New York: Raven Press; 1993:371-387.
37. Shibutani S, Takeshita M, Grollman AP: **Insertion of specific bases during DNA synthesis past the oxidation-damaged base 8-oxodG.** *Nature* 1991, **349**:431-434.
38. Moriya M: **Single-stranded shuttle phagemid for mutagenesis studies in mammalian cells: 8-oxoguanine in DNA induces targeted G.C-->T.A transversions in simian kidney cells.** *Proc Natl Acad Sci USA* 1993, **90**:1122-1126.
39. Kornyushyna O, Berges AM, Muller JG, Burrows CJ: **In vitro nucleotide misinsertion opposite the oxidized guanosine lesions spiroiminodihydantoin and guanidinohydantoin and DNA synthesis past the lesions using Escherichia coli DNA polymerase I (Klenow fragment).** *Biochemistry* 2002, **41**:15304-15314.
40. Cadet J, Berger M, Buchko GW, Joshi PC, Raoul S, Ravanat JL: **2,2-Diamino-4-[(3,5-di-O-acetyl-2-deoxy-.beta.-D-erythro- pentofuranosyl)amino]-5-(2H)-oxazolone: a Novel and Predominant Radical Oxidation Product of 3',5'-Di-O-acetyl-2'-deoxyguanosine.** *J Am Chem Soc* 1994, **116**:7403-7404.
41. Goyal RN, Jain N, Garg DK: **Electrochemical and enzymic oxidation of guanosine and 8-hydroxyguanosine and the effects of oxidation products in mice.** *Bioelectrochemistry and Bioenergetics* 1997, **43**:105-114.
42. Ye Y, Muller JG, Luo W, Mayne CL, Shallop AJ, Jones RA, Burrows CJ: **Formation of 13C-, 15N-, and 18O-labeled guanidinohydantoin from guanosine oxidation with singlet oxygen. Implications for structure and mechanism.** *J Am Chem Soc* 2003, **125**:13926-13927.
43. Burrows CJ, Muller JG, Kornyushyna O, Luo W, Duarte V, Leipold MD, David SS: **Structure and potential mutagenicity of new hydantoin products from guanosine and 8-oxo-7,8-dihydroguanine oxidation by transition metals.** *Environ Health Perspect* 2002, **110(Suppl 5)**:713-717.
44. Kino K, Sugiyama H: **UVR-induced G-C to C-G transversions from oxidative DNA damage.** *Mutat Res* 2005, **571**:33-42.
45. Kino K, Sugiyama H: **Possible cause of G-C-->C-G transversion mutation by guanine oxidation product, imidazolone.** *Chem Biol* 2001, **8**:369-378.
46. Kino K, Ito N, Sugasawa K, Sugiyama H, Hanaoka F: **Translesion synthesis by human DNA polymerase eta across oxidative products of guanine.** *Nucleic Acids Symp Ser* 2004, **48**:171-172.
47. Hailer MK, Slade PG, Martin BD, Sugden KD: **Nei deficient Escherichia coli are sensitive to chromate and accumulate the oxidized guanine lesion spiroiminodihydantoin.** *Chem Res Toxicol* 2005, **18**:1378-1383.
48. Matter B, Malejka-Giganti D, Csallany AS, Tretyakova N: **Quantitative analysis of the oxidative DNA lesion, 2,2-diamino-4-(2-deoxy-beta-D-erythro-pentofuranosyl)amino]-5(2H)-oxazolone (oxazolone), in vitro and in vivo by isotope dilution-capillary HPLC-ESI-MS/MS.** *Nucleic Acids Res* 2006, **34**:5449-5460.
49. Justice MJ, Noveroske JK, Weber JS, Zheng B, Bradley A: **Mouse ENU mutagenesis.** *Hum Mol Genet* 1999, **8**:1955-1963.
50. Rojas E, Lopez MC, Valverde M: **Single cell gel electrophoresis: methodology and applications.** *Journal of Chromatography B* 1999, **722**:225-254.
51. Park EJ, Yoon J, Choi K, Yi J, Park K: **Induction of chronic inflammation in mice treated with titanium dioxide nanoparticles by intratracheal instillation.** *Toxicology* 2009, **260**:37-46.
52. Kaewamatawong T, Shimada A, Okajima M, Inoue H, Morita T, Inoue K, Takano H: **Acute and subacute pulmonary toxicity of low dose of ultrafine colloidal silica particles in mice after intratracheal instillation.** *Toxicol Pathol* 2006, **34**:958-65.
53. Sasaki YF, Tsuda S, Izumiyama F, Nishidate E: **Detection of chemically induced DNA lesions in multiple mouse organs (liver, lung, spleen, kidney, and bone marrow) using the alkaline single cell gel electrophoresis (Comet) assay.** *Mutat Res* 1997, **388**:33-44.
54. Toyoizumi T, Deguchi Y, Masuda S, Kinae N: **Genotoxicity and estrogenic activity of 3,3'-dinitrobisphenol A in goldfish.** *Biosci Biotechnol Biochem* 2008, **72**:2118-2123.
55. Nohmi T, Suzuki T, Masumura K: **Recent advances in the protocols of transgenic mouse mutation assays.** *Mutat Res* 2000, **455**:191-215.

Mutation Research 673 (2009) 74–77

Contents lists available at ScienceDirect

Mutation Research/Genetic Toxicology and Environmental Mutagenesis

journal homepage: www.elsevier.com/locate/gentox
Community address: www.elsevier.com/locate/mutres

Short communication

# Increased formation of gastric $N^2$-ethylidene-2′-deoxyguanosine DNA adducts in aldehyde dehydrogenase-2 knockout mice treated with ethanol

Haruna Nagayoshi[a,b], Akiko Matsumoto[c], Ryuhei Nishi[b], Toshihiro Kawamoto[d], Masayoshi Ichiba[c], Tomonari Matsuda[b,*]

[a] Osaka Prefectural Institute of Public Health, Osaka 537-0025, Japan
[b] Research Center for Environmental Quality Management, Kyoto University, Otsu 520-0811, Japan
[c] Department of Social and Environmental Medicine, Saga University, Saga 849-8501, Japan
[d] Department of Environmental Health, University of Occupational and Environmental Health, Kitakyusyu, Fukuoka 807-8555, Japan

ARTICLE INFO

*Article history:*
Received 2 September 2008
Received in revised form 7 October 2008
Accepted 22 November 2008
Available online 3 December 2008

*Keywords:*
*Aldh2* knock-out mouse
Acetaldehyde
Stomach
LC/MS/MS
$N^2$-Ethylidene-2′-deoxyguanosine
$N^2$-Ethyl-2′-deoxyguanosine

ABSTRACT

We analyzed an acetaldehyde-derived DNA adduct, $N^2$-ethylidene-2′-deoxyguanosine ($N^2$-Eti-dG) in stomach DNA of aldehyde dehydrogenase (*Aldh*)-*2*-knockout mice that were fed with alcohol to determine effects of alcohol consumption and *Aldh2* genotype on the level of DNA damage in stomach. *Aldh2*-active(+/+), heterozygote(+/−) and knockout(−/−) mice were fed 20% ethanol for 5 weeks, then the level of $N^2$-Eti-dG in stomach was determined by liquid chromatography tandem mass spectrometry. The average $N^2$-Eti-dG level in DNA from untreated mice was not significantly different among *Aldh2* genotypes (2.0–3.1 adducts/$10^7$ bases), however, the average $N^2$-Eti-dG level in DNA from ethanol-treated mice was $4.8 \pm 2.6$ adducts/$10^7$ bases in *Aldh2*+/+ mice, $7.9 \pm 1.1$ adducts/$10^7$ bases in *Aldh2*+/− mice, and $48.6 \pm 12.0$ adducts/$10^7$ bases in *Aldh2*−/− mice, respectively. Our data clearly showed that alcohol drinking caused DNA damage in stomach, which was *Aldh2* genotype-dependent in this experimental animal model. This result suggests that heavy-alcohol drinking and *Aldh2* deficiency might be risk factors of stomach cancer.


## 1. Introduction

Alcohol intake is a risk factor for several types of cancer. Many studies of different design and in different populations around the world have consistently shown that daily alcohol consumption is a risk factor for cancers of oral cavity, pharynx, larynx and oesophagus [1–3]. Daily consumption of around 50 g of ethanol increases the risk for these cancers two to three times [1]. Moreover, many epidemiological studies consistently suggested that alcohol consumption is associated with an increased risk of liver cancer, breast cancer and colorectal cancer. In the case of stomach cancer, although many studies failed to show evidence of an association between alcohol drinking and stomach cancer risk, there are several other studies that clearly showed an association [4–7]. Endoscopic screening has yielded a higher rate of detection of gastric carcinoma in alcoholic Japanese men (1.7%) than in the general male Japanese population (0.2%) [8].

When the alcohol is assimilated, ethanol is metabolized and excreted in two steps. Firstly, ethanol is oxidized to acetaldehyde by alcohol dehyderogenase (ADH) and the ADH holoenzyme may exist as either a homodimer or heterodimer of α, β and γ subunits, encoded by *ADH1A*, *ADH1B* and *ADH1C*. The second step is the oxidation of acetaldehyde to acetate by aldehyde dehydrogenase (ALDH) or inducible cytochrome P450 2E1. Among human ALDH isozymes, the Michaelis constant ($K_m$) value of mitochondrial ALDH2 is predominantly low and that is why ALDH2 is a key enzyme for acetaldehyde metabolism. ALDH2 is a homotetrameric enzyme and the protein encoded by *ALDH2*2* has glutamic acid to lysin substitution at residue 487, resulting in an inactive subunit and dysfunctional ALDH2. ALDH2 has three types of polymorphism: *ALDH2*1/2*1*, an active form; *ALDH2*1/2*2*, a deficient form and *ALDH2*2/2*2* an inactive form. In *ALDH2*1/2*2* or *ALDH2*2/2*2* individuals, aldehyde remains in the body longer than in active *ALDH2*1/2*1* individuals and carcinogenic potential of acetaldehyde is exhibited [2,9].

Several reports described association between *ALDH2* genetic polymorphism and gastric cancers. Yokoyama and his colleagues reported that *ALDH2* genetic polymorphism was closely related with gastric cancer risk in Japanese alcoholic patients [10–12]. Chronic atrophic gastritis (CAG), which in many cases is induced

*Abbreviations:* ADH, alcohol dehydrogenase; ALDH, aldehyde dehydrogenase; $N^2$-Eti-dG, $N^2$-ethylidene-2′-deoxyguanosine; $N^2$-Et-dG, $N^2$-ethyl-2′-deoxyguanosine; CAG, chronic atrophic gastritis; α-*S*-Me-γ-OH-PdG, α-*S*-methyl-γ-hydroxy-1, $N^2$-propano-2′-deoxyguanosine; α-*R*-Me-γ-OH-PdG, α-*R*-methyl-γ-hydroxy-1, $N^2$-propano-2′-deoxyguanosine; 8-oxo-dG, 8-oxo-7,8-dihydro-2′-deoxyguanosine; LC/MS/MS, liquid chromatography tandem mass spectrometry.

* Corresponding author. Tel.: +81 75 753 5052; fax: +81 75 753 5052.
*E-mail address:* matsuda@z05.mbox.media.kyoto-u.ac.jp (T. Matsuda).

1383-5718/$ – see front matter © 2008 Elsevier B.V. All rights reserved.
doi:10.1016/j.mrgentox.2008.11.009

by *Helicobacter pylori* infection, and *ALDH2*1/2*2* are independently associated with increase of gastric cancer risk in Japanese alcoholic patients. Combinations of CAG and *ALDH2*1/2*2* showed greater risks of gastric carcinoma (*OR* = 39.2 for severe CAG plus *ALDH2*1/2*2*, CAG negative plus *ALDH2*1/2*1* was used as a reference) [11]. Zhang et al. also reported that another polymorphism of *ALDH2* found in Europeans, *ALDH2* Ex1 + 82A > *G*, is associated with alcohol-related increase in gastric cancer risk in Poland, although biochemical properties of this new polymorphism are not well understood [13]. These data suggest that acetaldehyde plays crucial roles in the development of stomach cancers.

Acetaldehyde is thought to be a tumor initiator because of its mutagenic and DNA-damaging properties [14–17]. Acetaldehyde forms several DNA adducts such as $N^2$-ethyl-2′-deoxyguanosine ($N^2$-Et-dG), α-*S*- and α-*R*-methyl-γ-hydroxy-1, $N^2$-propano-2′-deoxyguanosine (α-*S*-Me-γ-OH-PdG and α-*R*-Me-γ-OH-PdG) [18–20]. Aside from these stable DNA adducts, reaction of acetaldehyde results in the formation of an unstable and more abundant DNA adduct, $N^2$-ethylidene-dG ($N^2$-Eti-dG). Wang et al. showed that $N^2$-Eti-dG in human liver DNA is relatively stable and that the presence of this adduct could be confirmed by detection of $N^2$-Et-dG after reduction of DNA during isolation and enzymatic hydrolysis [21]. Because $N^2$-Eti-dG is the most abundant DNA adduct among acetaldehyde-derived adducts, it would be the sensitive biomarker of acetaldehyde exposure. In this study, we analyzed $N^2$-Eti-dG in stomach DNA of *Aldh2*-knockout mice that were exposed to alcohol to determine the effects of alcohol consumption and *Aldh2* genotype on the level of DNA damage in the stomach.

## 2. Materials and methods

### 2.1. Animal treatment

10–11-week old male *ALDH2*-knockout mice, which had been backcrossed C57BL6, were obtained from the Department of Environmental Health, University of Occupational and Environmental Health, Japan. The mice were used in conformity with the regulation of the committee on animal experiments of Saga University, Japan. The genotype of *ALDH2* was determined by polymerase chain reaction according to the method of Kitagawa et al. using genomic DNA from their ears and lungs [22].

The mice were fed 20% ethanol solution and standard hard feed CR-LPF (348 kcal/100 g) (Charles River Japan, Yokohama, Japan) for 5 weeks. They were then killed and stomach tissue specimens were collected, frozen in liquid nitrogen and stored at −80 °C until they were analyzed.

### 2.2. DNA isolation from mice stomach

For quantification of 8-oxo-7,8-dihydro-2′-deoxyguanosine (8-oxo-dG), mouse stomach DNA was extracted and purified by using Gentra® puregene™ tissue kit (QIAGEN). The protocol was performed basically as per manufacture's instructions except that desferroxamine (final concentration: 0.1 mM) was added to all solutions to avoid formation of oxidative adducts during the purification step.

For quantification of $N^2$-Eti-dG, DNA was isolated as described previously [23]. Gentra Puregen tissue kit was used. The procedure was basically as per manufacture's instructions except for adding $NaBH_3CN$ to all solutions (final concentration: 100 mM). After the purification step, DNA was dissolved in 10 mM Tris–HCl/5 mM EDTA buffer (pH 7.0), extracted with chloroform and precipitated with ethanol.

### 2.3. DNA adduct standards and their stable isotope

8-oxo-dG was purchased from Sigma–Aldrich Japan, Tokyo, Japan. [U-$^{15}N_5$] 8-oxo-dG was kindly supplied by Dr. Shibutani at SUNY Stony Brook, USA. $N^2$-Et-dG and its [U-$^{15}N_5$]-labeled standard was synthesized as described previously [18].

### 2.4. DNA digestion

20 μg aliquots of DNA were digested into their constituent 2′-deoxyribonucleoside-3′-monophosphate units by the addition of 15 μl of 17 mM citrate plus 8 mM $CaCl_2$ buffer that contained micrococcal nuclease (22.5 U) and spleen phosphodiesterase (0.075 U) plus internal standards. The solutions were mixed and incubated for 3 h at 37 °C, after which alkaline phosphatase (1 U), 10 μl of 0.5 M Tris–HCl (pH 8.5), 5 μl of 20 mM $ZnSO_4$ and 67 μl of distilled water were added and incubated for a further 3 h at 37 °C. The digested sample was extracted twice with methanol. The methanol fractions were evaporated to dryness, resuspended in 50 μl of distilled water and subjected to liquid chromatography tandem mass spectrometry (LC/MS/MS).

### 2.5. Instrument

LC/MS/MS analyses were performed using a Shimadzu LC system (Shimadzu, Kyoto, Japan) interfaced with a Quattro Ultima triple stage quadrupole MS (Waters-Micromass, Manchester, UK). The LC column was eluted over a gradient that began at a ratio of 5% methanol to 95% water and was changed to 40% methanol over a period of 30 min, changed to 80% methanol from 30 to 35 min and finally returned to the original starting conditions, 5:95, for the remaining 11 min. The total run time was 46 min. Sample injection volumes of 20 μl each were separated on a Shim-pack XR-ODS column (3.0 mm × 75 mm, 2.2 μm) and eluted at a flow rate of 0.2 ml/min. Mass spectral analyses were carried out in positive ion mode with nitrogen as the nebulizing gas. The ion source temperature was 130 °C, the desolvation gas temperature was 380 °C and the cone voltage was operated at a constant 35 V. Nitrogen gas was also used as the desolvation gas (700 l/h) and cone gas (35 l/h) and argon was used to provide a collision cell pressure of $1.5 \times 10^{-3}$ mbar. Positive ions were acquired in multiple reaction monitoring (MRM) mode. The MRM transitions monitored were as follows: [$^{15}N_5$]8-oxo-dG, *m/z* 288 → 172; 8-oxo-dG, *m/z* 283 → 167; [$^{15}N_5$] $N^2$-Et-dG, *m/z* 301 → 185 and $N^2$-Et-dG, *m/z* 295.5 → 179.9. The amount of each adduct was quantified by the ratio of the peak area of the target adducts to that of its stable isotope. Quanlynx (version 4.0) software (Waters-Micromass) was used to create standard curves and to calculate adduct concentrations. The amount of deoxyguanosine was monitored at 254 nm by a Shimadzu SPD-10A UV-Visible detector that was in place before the tandem MS.

## 3. Results

The mice were fed with water or 20% ethanol and standard hard feed for 5 weeks. Feed intake slightly dropped in the 20% ethanol group, but there was no significant difference amongst the *Aldh2* genotypes. The average ethanol intake in the case of the 20% ethanol group was not significantly different between *Aldh2* genotypes (~23 g/day/kg body wt). Reduction in body weight was observed predominantly in *Aldh2*−/− mice as described in our previous report [24]. After 5 weeks of feeding with water and 20% ethanol, the mice were killed and their stomach DNA was extracted and purified to detect DNA adduct level.

Firstly, we analyzed the level of acetaldehyde-inducible stable DNA adducts, $N^2$-Et-dG. However, it was not detected in any stomach DNA samples for both alcohol-treated and non-treated mice for any *Aldh2* genotype. Next, to determine acetaldehyde-derived major DNA adduct, $N^2$-Eti-dG in DNA, we purified stomach DNA using several reagents containing strong reducing agent, $NaBH_3CN$. During the purification procedure, it was expected that $N^2$-Eti-dG would be converted to stable $N^2$-Et-dG (Fig. 1). The average $N^2$-Eti-dG level in DNA from untreated mice was 3.1 ± 2.3 adducts/$10^7$ bases in *Aldh2*+/+ mice, 2.0 ± 0.6 in *Aldh2*+/− mice, and 2.2 ± 0.4 in *Aldh2*−/− mice, respectively. On the other hand, in 20% ethanol-treated mice, significant $N^2$-Eti-dG level increase was observed. The average $N^2$-Eti-dG level in DNA from 20% ethanol-treated mice was 4.8 ± 2.6 adducts/$10^7$ bases in *Aldh2*+/+ mice, 7.9 ± 1.1 adducts/$10^7$ bases in *Aldh2*+/− mice, and 48.6 ± 12.0 adducts/$10^7$ bases in *Aldh2*−/− mice, respectively (Fig. 2A). This data indicated that *Aldh2* genotype has an effect on gastric $N^2$-Eti-dG level. On the other hand, DNA adduct induced by oxidative stress, 8-oxo-dG, was detected in all samples, but neither alcohol-dependent nor *Aldh2* genotype-dependent change was observed (Fig. 2B).

## 4. Discussion

Several epidemiological evidences suggested that alcohol consumption is a risk factor of gastric cancer and genotype of *ALDH2* is considered to play an important role in increasing the risk. One animal carcinogenicity study supported the epidemiological observation. Male and female Sprague–Dawley rats fed on 10% ethanol, started at 39 weeks of age and continued until their spontaneous death, showed significantly increased frequency of forestomach

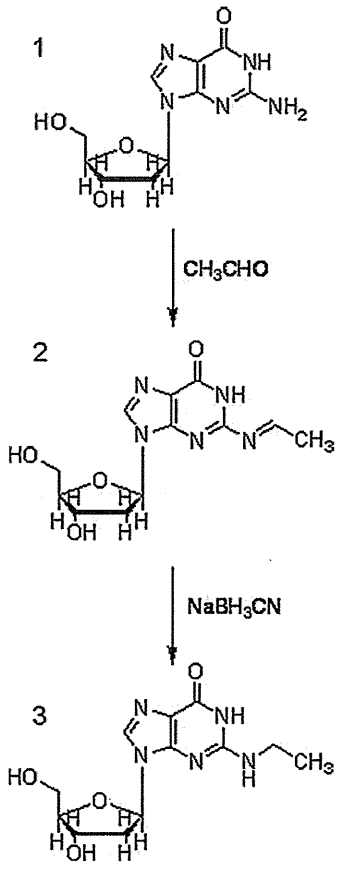


**Fig. 1.** Formation of acetaldehyde-dG adducts: (1) 2′-deoxyguanosine; (2) $N^2$-ethylidene-2′-deoxyguanosine ($N^2$-Eti-dG); (3) $N^2$-ethyl-2′-deoxyguanosine ($N^2$-Et-dG) $N^2$-Eti-dG was easily reduced with $NaBH_3CN$.

acanthoma and carcinoma [25]. However, little other experimental evidence, which support the relationship between *ALDH2* genotype and gastric cancer risk, was available. In this study, we clearly showed that ethanol significantly induced $N^2$-Eti-dG DNA adducts in mouse stomach, and formation of the DNA adduct was *Aldh2* genotype-dependent. This result is consistent with the report by Ogawa et al. which showed *Aldh2* genotype-dependent incorporation of radioactivity in stomach DNA of mice administered $^3H$- or $^{14}C$-labeled ethanol [26].

Several pathways are considered for generation of and exposure to acetaldehyde in stomach. A portion of consumed ethanol is absorbed through stomach mucosa. ADH1C is the major ADH expressed in stomach mucosa, and a portion of absorbed ethanol should be metabolized to acetaldehyde on site [9,27]. Ethanol, absorbed from digestive organs, is distributed throughout the body and the majority of it is metabolized in liver where most of the ADHs are expressed (ADH1A, ADH1B, ADH1C, ADH2, ADH3, ADH4 and ADH5) [9], and produced acetaldehyde is distributed throughout the body via circulation, and the stomach may be exposed to acetaldehyde via circulatory fluids. Another important pathway is via saliva. Ethanol contained in saliva is metabolized to acetaldehyde by oral flora [28], and the upper digestive tract, including the stomach, is continuously expose to saliva with high concentration of acetaldehyde.

The concentration of acetaldehyde in saliva after ingesting ethanol is much higher than in blood, and the acetaldehyde concentration in saliva is significantly higher in *ALDH2* deficient individuals than in normal individuals [29,30]. Alcohol challenge test of 0.6 g ethanol/kg body weight of healthy human volunteers resulted in peak acetaldehyde concentration in blood and saliva of 5 and 53 μM, respectively in *ALDH2*1/*1* homozygotes and 25 and 76 μM, respectively in *ALDH2*1/*2* heterozygotes [29]. Taking this into consideration, in this study, the stomach is considered to be exposed to higher concentration of acetaldehyde in *Aldh2*(−/−) mice than *Aldh2*(+/+) mice via both fluid and saliva pathways.

Human stomach mucosa expresses ALDH1, ALDH2 and ALDH3. The most abundant one is ALDH3, however, its $K_m$ value is thought to be several orders of magnitude higher than that of ALDH2 [26,31]. Klyosov et al. reported that the $K_m$ value of human ALDH1, ALDH2 and hamster ALDH3 were 180 μM, 200 nM and 3.6 mM, respectively when acetaldehyde was used as a substrate [32]. Considering realistic blood and salivary acetaldehyde concentration, ALDH3 may not work well in the stomach, and ALDH2 as well as ALDH1 will con-

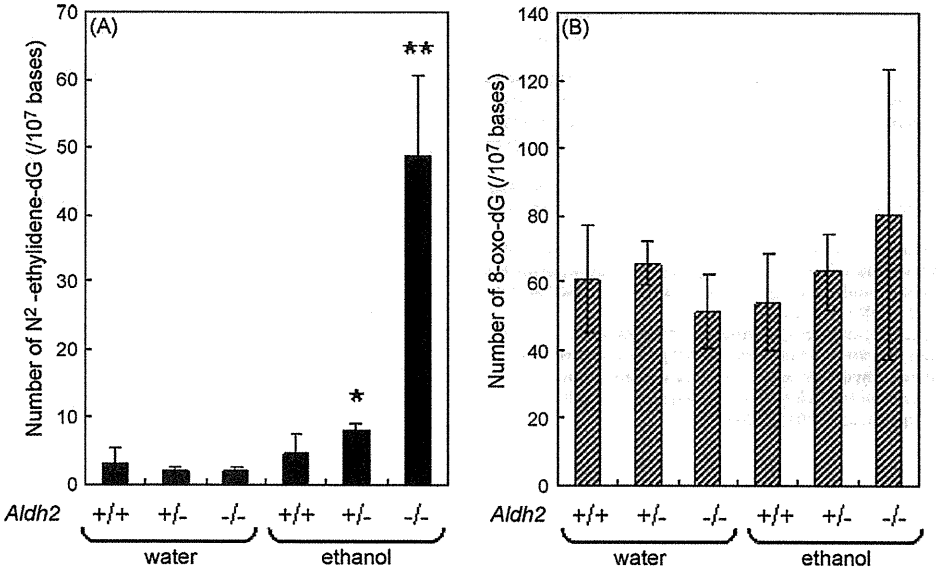


**Fig. 2.** DNA adduct levels in control and alcohol-treated mice having different *Aldh2* genotypes. Mice were fed with water (*Aldh2*+/+: $n=5$, (+/−): $n=6$, (−/−): $n=5$) or 20% ethanol (*Aldh2*+/+: $n=6$, (+/−): $n=5$, (−/−): $n=4$) for 5 weeks. Stomach DNA samples were purified with $NaBH_3CN$ for the determination of $N^2$-Eti-dG or without $NaBH_3CN$ for the determination of 8-oxo-dG. Unstable $N^2$-Eti-dG was reduced to stable $N^2$-Et-dG under the presence of $NaBH_3CN$. The level of $N^2$-Eti-dG was detected as $N^2$-Et-dG by LC/MS/MS. (A) Shows the levels of $N^2$-Eti-dG in mice stomach DNA and (B) shows the level of 8-oxo-dG in mice stomach. The error bars represent the standard deviation. (*) Significantly increased from water control (+/−); (**) significantly increased from water control (−/−) or ethanol-treated *Aldh2*+/+ mice ($p<0.01$).

tribute to the clearance of acetaldehyde in stomach mucosa. In this situation again, high concentration of acetaldehyde should remain longer in the stomach in *Aldh2*(−/−) mice than in *Aldh2*(+/+) mice.

In conclusion, our data clearly showed that alcohol drinking caused DNA damage in the stomach, and the risk was *ALDH2* genotype-dependent. This strongly supports the epidemiological observations which suggest alcohol drinking and *ALDH2* deficiency are risk factors of stomach cancers.

## Conflicts of interest

The authors declare that there are no conflicts of interest.

## Acknowledgments

This research was supported in part by Grants-in-aid for Cancer Research from the Ministry of Health, Labor and Welfare of Japan and Grants-in-aid for Scientific Research from the Ministry of Education, Culture, Sports, Science and Technology of Japan. This research was also supported in part by Encouragement of Young Scientists from the Ministry of Education, Culture, Sports, Science and Technology of Japan and by Suntory Limited.

## References

[1] R. Baan, K. Straif, Y. Grosse, B. Secretan, F. El Ghissassi, V. Bouvard, A. Altieri, V. Cogliano, Carcinogenicity of alcoholic beverages, Lancet Oncol. 8 (2007) 292–293.
[2] H.K. Seitz, F. Stickel, Molecular mechanisms of alcohol-mediated carcinogenesis, Nat. Rev. Cancer 7 (2007) 599–612.
[3] International Agency for Research on Cancer, IARC monographs on the evaluation of carcinogenic risks to humans Consumption of Alcoholic Beverages and Ethyl Carbamate (Urethane), Summaries and Evaluation, vol. 96, 2007, http://monographs.iarc.fr/ENG/Meetings/96-alcohol.pdf.
[4] T. Shimazu, I. Tsuji, M. Inoue, K. Wakai, C. Nagata, T. Mizoue, K. Tanaka, S. Tsugane, Alcohol drinking and gastric cancer risk: an evaluation based on a systematic review of epidemiologic evidence among the Japanese population, Jpn. J. Clin. Oncol. 38 (2008) 8–25.
[5] T. Ubukata, M. Nakao, A. Ohshima, T. Sobue, H. Tsukuma, K. Morinaga, et al., Drinking and smoking in the etiology of stomach cancer, Nippon Koshu Eisei Zasshi 35 (1988) 286–292 (in Japanese).
[6] I. Kato, S. Tominaga, Y. Ito, S. Kobayashi, Y. Yoshii, A. Matsuura, A. Kameya, T. Kano, A. Ikari, A prospective study of atrophic gastritis and stomach cancer risk, Jpn. J. Cancer Res. 83 (1992) 1137–1142.
[7] S. Kikuchi, T. Nakajima, O. Kobayashi, T. Yamazaki, M. Kikuichi, K. Mori, S. Oura, H. Watanabe, H. Nagawa, R. Otani, N. Okamoto, M. Kurosawa, H. Anzai, T. Konishi, S. Futagawa, N. Mizobuchi, O. Kobori, R. Kaise, Y. Inaba, O. Wada, U-shaped effect of drinking and linear effect of smoking on risk for stomach cancer in Japan, Jpn. J. Cancer Res. 93 (2002) 953–959.
[8] A. Yokoyama, T. Ohmori, T. Muramatsu, S. Higuchi, T. Yokoyama, S. Matsushita, M. Matsumoto, K. Maruyama, M. Hayashida, H. Ishii, Cancer screening of upper aerodigestive tract in Japanese alcoholics with reference to drinking and smoking habits and aldehyde dehydrogenase-2 genotype, Int. J. Cancer 68 (1996) 313–316.
[9] W. Jelski, M. Szmitkowski, Alcohol dehydrogenase (ADH) and aldehyde dehydrogenase (ALDH) in the cancer diseases, Clin. Chim. Acta 395 (2008) 1–5.
[10] A. Yokoyama, T. Muramatsu, T. Omori, T. Yokoyama, S. Matsushita, S. Higuchi, K. Maruyama, H. Ishii, Alcohol and aldehyde dehydrogenase gene polymorphisms and oropharyngolaryngeal, esophageal and stomach cancers in Japanese alcoholics, Carcinogenesis 22 (2001) 433–439.
[11] A. Yokoyama, T. Yokoyama, T. Omori, S. Matsushita, T. Mizukami, H. Takahashi, S. Higuchi, K. Maruyama, H. Ishii, T. Hibi, *Helicobacter pylori*, chronic atrophic gastritis, inactive aldehyde dehydrogenase-2, macrocytosis and multiple upper aerodigestive tract cancers and the risk for gastric cancer in alcoholic Japanese men, J. Gastroenterol. Hepatol. 22 (2007) 210–217.
[12] A. Yokoyama, T. Muramatsu, T. Ohmori, T. Yokoyama, K. Okuyama, H. Takahashi, Y. Hasegawa, S. Higuchi, K. Maruyama, K. Shirakura, H. Ishii, Alcohol-related cancers and aldehyde dehydrogenase-2 in Japanese alcoholics, Carcinogenesis 19 (1998) 1383–1387.
[13] F.F. Zhang, L. Hou, M.B. Terry, J. Lissowska, A. Morabia, J. Chen, M. Yeager, W. Zatonski, S. Chanock, W.H. Chow, Genetic polymorphisms in alcohol metabolism, alcohol intake and the risk of stomach cancer in Warsaw, Poland, Int. J. Cancer 121 (2007) 2060–2064.
[14] P.J. Brooks, J.A. Theruvathu, DNA adducts from acetaldehyde: implications for alcohol-related carcinogenesis, Alcohol 35 (2005) 187–192.
[15] T. Matsuda, M. Kawanishi, T. Yagi, S. Matsui, H. Takebe, Specific tandem GG to TT base substitutions induced by acetaldehyde are due to intra-strand crosslinks between adjacent guanine bases, Nucleic Acids Res. 26 (1998) 1769–1774.
[16] T. Matsuda, I. Terashima, Y. Matsumoto, H. Yabushita, S. Matsui, S. Shibutani, Effective utilization of $N^2$-ethyl-2′-deoxyguanosine triphosphate during DNA synthesis catalyzed by mammalian replicative DNA polymerases, Biochemistry 38 (1999) 929–935.
[17] I. Terashima, T. Matsuda, T.W. Fang, N. Suzuki, J. Kobayashi, K. Kohda, S. Shibutani, Miscoding potential of the $N^2$-ethyl-2′-deoxyguanosine DNA adduct by the exonuclease-free Klenow fragment of *Escherichia coli* DNA polymerase I, Biochemistry 40 (2001) 4106–4114.
[18] J.L. Fang, C.E. Vaca, Detection of DNA adducts of acetaldehyde in peripheral white blood cells of alcohol abusers, Carcinogenesis 18 (1997) 627–632.
[19] M. Wang, E.J. McIntee, G. Cheng, Y. Shi, P.W. Villalta, S.S. Hecht, Identification of DNA adducts of acetaldehyde, Chem. Res. Toxicol. 13 (2000) 1149–1157.
[20] T. Matsuda, H. Yabushita, R.A. Kanaly, S. Shibutani, A. Yokoyama, Increased DNA damage in ALDH2-deficient alcoholics, Chem. Res. Toxicol. 19 (2006) 1374–1378.
[21] M. Wang, N. Yu, L. Chen, P.W. Villalta, J.B. Hochalter, S.S. Hecht, Identification of an acetaldehyde adduct in human liver DNA and quantitation as $N^2$-ethyldeoxyguanosine, Chem. Res. Toxicol. 19 (2006) 319–324.
[22] K. Kitagawa, T. Kawamoto, N. Kunugita, T. Tsukiyama, K. Okamoto, A. Yoshida, K. Nakayama, Aldehyde dehydrogenase (ALDH) 2 associates with oxidation of methoxyacetaldehyde; in vitro analysis with liver subcellular fraction derived from human and *Aldh2* gene targeting mouse, FEBS Lett. 476 (2000) 306–311.
[23] T. Matsuda, A. Matsumoto, M. Uchida, R.A. Kanaly, K. Misaki, S. Shibutani, T. Kawamoto, K. Kitagawa, K.I. Nakayama, K. Tomokuni, M. Ichiba, Increased formation of hepatic $N^2$-ethylidene-2′-deoxyguanosine DNA adducts in aldehyde dehydrogenase 2-knockout mice treated with ethanol, Carcinogenesis 28 (2007) 2363–2366.
[24] A. Matsumoto, T. Kawamoto, F. Mutoh, T. Isse, T. Oyama, K. Kitagawa, K.I. Nakayama, M. Ichiba, Effects of 5-week ethanol feeding on the liver of aldehyde dehydrogenase 2 knockout mice, Pharmacogenet. Genomics 18 (2008) 847–852.
[25] M. Soffritti, F. Belpoggi, D. Cevolani, M. Guarino, M. Padovani, C. Maltoni, Results of long-term experimental studies on the carcinogenicity of methyl alcohol and ethyl alcohol in rats, Annu. N. Y. Acad. Sci. 982 (2002) 46–69.
[26] M. Ogawa, T. Oyama, T. Isse, K. Saito, Y. Tomigahara, Y. Endo, T. Kawamoto, A comparison of covalent binding of ethanol metabolites to DNA according to *Aldh2* genotype, Toxicol. Lett. 168 (2007) 148–154.
[27] S.J. Yin, T.C. Cheng, C.P. Chang, Y.J. Chen, Y.C. Chao, H.S. Tang, T.M. Chang, C.W. Wu, Human stomach alcohol and aldehyde dehydrogenases (ALDH): a genetic model proposed for ALDH III isozymes, Biochem Genet 26 (1988) 343–360.
[28] M. Muto, Y. Hitomi, A. Ohtsu, H. Shimada, Y. Kashiwase, H. Sasaki, S. Yoshida, H. Esumi, Acetaldehyde production by non-pathogenic *Neisseria* in human oral microflora: implications for carcinogenesis in upper aerodigestive tract, Int. J. Cancer 88 (2000) 342–350.
[29] S. Vakevainen, J. Tillonen, M. Salaspuro, 4-Methylpyrazole decreases salivary acetaldehyde levels in aldh2-deficient subjects but not in subjects with normal aldh2, Alcohol Clin. Exp. Res. 25 (2001) 829–834.
[30] A. Yokoyama, E. Tsutsumi, H. Imazeki, Y. Suwa, C. Nakamura, T. Mizukami, T. Yokoyama, Salivary acetaldehyde concentration according to alcoholic beverage consumed and aldehyde dehydrogenase-2 genotype, Alcohol Clin. Exp. Res. 32 (2008) 1607–1614.
[31] Y. Alnouti, C.D. Klaassen, Tissue distribution, ontogeny, and regulation of aldehyde dehydrogenase (Aldh) enzymes mRNA by prototypical microsomal enzyme inducers in mice, Toxicol. Sci. 101 (2008) 51–64.
[32] A.A. Klyosov, L.G. Rashkovetsky, M.K. Tahir, W.M. Keung, Possible role of liver cytosolic and mitochondrial aldehyde dehydrogenases in acetaldehyde metabolism, Biochemistry 35 (1996) 4445–4456.

*Published online 25 November 2009*

*Nucleic Acids Research, 2010, Vol. 38, No. 3* ***859–867***
*doi:10.1093/nar/gkp1095*

# Critical amino acids in human DNA polymerases η and κ involved in erroneous incorporation of oxidized nucleotides

**Atsushi Katafuchi[1], Akira Sassa[1,2], Naoko Niimi[1], Petr Grúz[1], Hirofumi Fujimoto[3], Chikahide Masutani[4], Fumio Hanaoka[5], Toshihiro Ohta[2] and Takehiko Nohmi[1,*]**

[1]Division of Genetics and Mutagenesis, National Institute of Health Sciences, 1-18-1 Kamiyoga, Setagaya-ku, Tokyo 158-8501, [2]School of Life Sciences, Tokyo University of Pharmacy and Life Sciences, Hachiouji-shi, Tokyo 192-0392, [3]Division of Radiological Protection and Biology, National Institute of Infectious Diseases, 1-23-1 Toyama, Shinjuku-ku, Tokyo 162-8640, [4]Graduate School of Frontier Biosciences, Osaka University and SORST, JST, 1-3 Yamada-oka, Suita, Osaka 565-0871 and [5]Faculty of Science, Gakushuin University, 1-5-1 Mejiro, Toshima-ku, Tokyo 171-8588, Japan

Received September 22, 2009; Revised and Accepted November 6, 2009

## ABSTRACT

**Oxidized DNA precursors can cause mutagenesis and carcinogenesis when they are incorporated into the genome. Some human Y-family DNA polymerases (Pols) can effectively incorporate 8-oxo-dGTP, an oxidized form of dGTP, into a position opposite a template dA. This inappropriate G:A pairing may lead to transversions of A to C. To gain insight into the mechanisms underlying erroneous nucleotide incorporation, we changed amino acids in human Polη and Polκ proteins that might modulate their specificity for incorporating 8-oxo-dGTP into DNA. We found that Arg61 in Polη was crucial for erroneous nucleotide incorporation. When Arg61 was substituted with lysine (R61K), the ratio of pairing of dA to 8-oxo-dGTP compared to pairing of dC was reduced from 660:1 (wild-type Polη) to 7:1 (R61K). Similarly, Tyr112 in Polκ was crucial for erroneous nucleotide incorporation. When Tyr112 was substituted with alanine (Y112A), the ratio of pairing was reduced from 11:1 (wild-type Polκ) to almost 1:1 (Y112A). Interestingly, substitution at the corresponding position in Polη, i.e. Phe18 to alanine, did not alter the specificity. These results suggested that amino acids at distinct positions in the active sites of Polη and Polκ might enhance 8-oxo-dGTP to favor the *syn* conformation, and thus direct its misincorporation into DNA.**

## INTRODUCTION

Reactive oxygen species (ROS) are constantly generated in cells during normal aerobic metabolism. The intracellular levels of ROS are further enhanced by exposure of cells to redox agents or ionizing radiation (1–3). To counteract the potential genotoxicity and cytotoxicity of ROS, cells possess a number of defense systems, e.g. low-molecular-weight scavengers, ROS-degrading enzymes and DNA repair. Nevertheless, some ROS molecules escape the defense systems and eventually damage nearby bio-molecules including DNA, proteins and membrane lipids. Therefore, ROS has been implicated in the etiology of human degenerative diseases, aging and cancer (4,5).

DNA precursors (dNTPs) in the cellular nucleotide pool are subject to oxidation by ROS (6,7). Oxidized forms of DNA precursors include 7,8-dihydro-8-oxo-dGTP (8-oxo-dGTP), 7,8-dihydro-8-oxo-dATP (8-oxo-dATP) and 1,2-dihydro-2-oxo-dATP (2-OH-dATP). These oxidized dNTPs cause various deleterious effects in cells. For example, 8-oxo-dGTP can be incorporated opposite a dA residue in the template strand during DNA replication; this can result in an A to C transversion (8). *Escherichia coli* mutants deficient in the *mutT* gene, whose gene product hydrolyzes 8-oxo-dGTP, display spontaneous A to C transversion rates that are over 1000 times higher than those in wild-type strains (9,10). Similarly, 2-OH-dATP can be incorporated opposite template dG, and this induces G to T transversions. *Escherichia coli* mutants deficient in the *orf135* gene, whose gene product hydrolyzes 2-OH-dATP, display higher spontaneous G to T transversion rates than the

*To whom correspondence should be addressed. Tel: +81 3 3700 9872; Fax: +81 3 3700 2348; Email: nohmi@nihs.go.jp

wild-type strains (11,12). In higher-order organisms, the human MTH1 gene product, a functional counterpart of the *E. coli* MutT protein, hydrolyzes 8-oxo-dGTP, 8-oxo-dATP and also 2-OH-dATP; in contrast, MutT does not hydrolyze 2-OH-dATP (13,14). Overexpression of hMTH1 reduced total cellular 8-oxo-dG levels in human cells and transgenic mice. This overexpression also suppressed genome instability in cells with defective mismatch repair mechanisms; in addition, it caused delayed cellular senescence, and ameliorated neuropathological and behavioral symptoms in mice that resembled those of Huntington's disease (15,16). Alternatively, suppression of hMTH1 expression induced genomic DNA damage and caused accelerated cellular senescence in human skin fibroblasts (17). Mice deficient in the *Mth1* gene exhibited increased tumorigenicity in the lung, liver and stomach compared to wild-type mice (18). Thus, the nucleotide pool is a critical target of intracellular ROS, and oxidized nucleotides, unless continuously eliminated, can induce a variety of cellular abnormalities.

To exert these adverse effects, oxidized dNTPs must be incorporated into the genome DNA. Actually, in culture medium, 8-oxo-dG is readily incorporated into the genome DNA upon phosphorylation in human cells (19). Interestingly, Y-family DNA polymerases (Pols), a novel family of Pols involved in translesion DNA synthesis (20), efficiently and almost exclusively incorporated 8-oxo-dGTP into the DNA chain opposite a template dA (21). This specificity for erroneous pairing appears to be conserved in all Y-family Pols from bacteria, Archea and humans that have been examined. In *E. coli*, two Y-family Pols, i.e. Pol IV (DinB) and Pol V (UmuD′C), were involved in the erroneous incorporation of 8-oxo-dGTP and 2-OH-dATP into DNA in the *sod fur* mutants. In these mutants, intracellular ROS levels were elevated and, hence, the rates of spontaneous A to C and G to T transversions were elevated (22). The human Y-family Polη efficiently paired 8-oxo-dGTP with template dA (23). The incorporation of 8-oxo-dGTP into the genome of phage M13 by human Polη *in vitro* induced A to C transversions and deletions (24). In human cells, 8-oxo-dGTP induced an increase in the frequency of A to C mutations in the *supF* gene; this mutation frequency was reduced with the suppression of REV1, Polη and Polζ expression (25).

It has been shown that 8-oxo-dG assumes the *anti* conformation when it pairs with dC, but it assumes the *syn* conformation when pairing with dA (26,27). Therefore, we hypothesized that certain amino acids in the active sites of the Y-family Pols might force 8-oxo-dGTP to assume the *syn* conformation. In this study, we tested this hypothesis by amino acid substitutions of two Y-family human polymerases, Polη and Polκ. We changed three amino acids that might affect the specificity for pairing 8-oxo-dGTP with a template dA (28). The first candidates for amino acid alterations were the 'steric gate' amino acids, i.e. phenylalanine 18 (F18) of Polη and tyrosine 112 (Y112) in Polκ. These amino acids distinguish dNTPs and rNTPs by sensing their 2′-OH-groups (29). We reasoned that the proximity of these amino acids to the incoming dNTPs might play a critical role in determining the conformation of 8-oxo-dGTP. The second candidate for an amino acid alteration was arginine 61 (R61) in human Polη. This is the counterpart of yeast R73, which is located adjacent to the base of the incoming dNTP and stabilize dNTPs during bypass DNA synthesis across cisplatin adducts and cyclobutane pyrimidine dimers (30). The arginine residue is conserved in yeast and humans, but not in other Y-family Pols, including Polκ. The third candidate for an amino acid alteration was isoleucine 48 (I48) in Polη, which is the counterpart of yeast I59. This residue is also located close to the base of the dNTPs in the active site (30). Our results suggested that R61 in Polη and Y112 in Polκ were critical for the preferential pairing of 8-oxo-dGTP with template dA. This implies that distinctly positioned amino acids in the active sites of two Y-family Pols direct the conformation of the incoming 8-oxo-dGTP to the *syn* conformation. We discuss how R61 modulates the conformation of the incoming 8-oxo-dGTP in the active site of Polη.

## MATERIALS AND METHODS

### Substrates and enzymes

All oligonucleotides were purchased from BEX Corp. (Tokyo). Unaltered dNTPs were purchased from GE-Healthcare and oxidized dNTPs, i.e. 8-oxo-dGTP and 8-oxo-dATP, were purchased from TriLink BioTechnologies. 2-OH-dATP was kindly provided by Dr H. Kamiya (Hokkaido University). Human Polκ and the mutant Polκ with an alanine substitution at Y112 (Y112A) were prepared as described previously (31). The human Polη mutant enzymes included substitutions at F18 with alanine (F18A), at R61 with alanine, methionine, asparagine, glutamine, histidine or lysine (R61A, R61M, R61N, R61Q, R61H or R61K), and at I48 with serine, methionine, phenylalanine, asparagine or glutamine (I48S, I48M, I48F, I48N or I48Q). Polη and its mutant proteins were prepared with the pET21bXPV(1-511) plasmid that carried the human Polη cDNA sequence. Site-directed mutagenesis protocols were used to exchange the DNA sequences that encoded the targeted amino acids (QuickChange Lightening Site-Directed Mutagenesis Kit; STRATAGENE). The resulting plasmids were transformed into Rosetta (DE3) plysS cells (Novagen). The cells were grown in 1 l of Luria–Bertani (LB) medium until the cell density reached an $OD_{600} = 0.6$. The expression of Polη and the mutant proteins were induced with the addition of 0.2 mM IPTG at 15°C for 10 h (32). The resulting cell pastes were resuspended in lysis buffer comprised of 50 mM potassium phosphate buffer pH 7.0, 500 mM NaCl, 10% sucrose, 20% glycerol, 1× BugBuster (Novagen), 5 mM imidazole, 5 mM β-mercaptoethanol, benzonase nuclease (Novagen) and complete EDTA-free, which is a protease inhibitor cocktail (Roche). The resuspended mixtures were incubated on ice for 30 min. The lysates were clarified by centrifugation at 20 000*g* for 20 min at 4°C. TALON super flow metal affinity resin (Clontech) was washed twice with

wash buffer (50 mM potassium phosphate buffer pH 7.0, 500 mM NaCl, 10% glycerol, 10 mM imidazole, 5 mM β-mercaptoethanol, complete EDTA-free), and the washed resin was gently mixed with the supernatant containing the Polη or the mutant proteins for 30 min. After three subsequent washings, the resins were placed on the column, and washed twice. The Polη and the mutant proteins were eluted with 5 ml of elution buffer (the wash buffer plus 350 mM imidazole). For kinetics analyses, the proteins were further purified with HiLoad 16/60 Superdex 200 pg and HiTrap Heparin HP columns (both from GE Healthcare) with an FPLC system (AKTAexplorer 10 s, GE Healthcare). The pooled fractions containing wild-type hPolη, R61A and R61K were dialyzed against 25 mM Tris–HCl pH 7.5, 2.5 mM β-mercaptoethanol and 50% glycerol. All purified proteins were stored at −80°C.

### Incorporation of oxidized dNTPs

DNA extension assays were performed to test the behavior of the native and mutant Pols. The DNA primers used in the DNA extension assays were annealed with the template DNA sequence (5′-GAAGG GATCCTTAAGACNGTAACCGGTCTTCGCGCG-3′, where N represents A, C, G or T) at a molar ratio of 1 : 1.2. The template/primer (100 nM) was combined with appropriate concentrations of Polη (5 nM), Polκ (10 nM) and mutant proteins (5, 50 or 100 nM), and incubated in a reaction buffer [40 mM Tris–HCl (pH 8.0), 5 mM $MgCl_2$, 10 mM dithiothreitol, 100 μg/ml BSA, 60 mM KCl, 2.5% glycerol] with 50 μM of oxidized dNTPs for 10 min at 37°C. The exact concentrations of proteins are described in legends of figures and Supplementary Figures. Reactions were terminated by addition of the termination buffer (98% formamide, 10 mM EDTA, 10 mg/ml Blue dextran). After heat denaturation, the mixtures were loaded onto a denaturing 15% polyacrylamide gel for electrophoresis (PAGE), and run with a buffer containing 8 M urea. The products were visualized with a Molecular Imager FX Pro System (Bio-Rad Laboratories) and quantified with Quantity One software (Bio-Rad Laboratories). For steady-state kinetic analyses of incorporation of oxidized dNTP, the reactions were carried out with 1 nM Polη and 5 nM Polκ. Both the concentrations of dNTP and the incubation times were varied according to the activity of a given enzyme. The products were analyzed as described in the primer extension assay. The rate of incorporation was plotted against dNTP concentrations, and the apparent Michaelis–Menten constant, $K_m$ and $V_{max}$ values were determined by Enzyme Kinetics Module 1.1 of SigmaPlot 2001 software (SPSS Inc., IL). The $k_{cat}$ was calculated by dividing the $V_{max}$ by the enzyme concentration. All values represent means plus standard errors from three independent experiments.

### Translesion DNA synthesis assay

Primer DNA (5′-CTTCCCTAGGAATTCTGC-3′) labeled with Cy3 at the 5′-end was annealed to template DNA (5′-GCGCGCTTCTGGCCAATXGCAGAATTC CTAGGGAAG-3′, where X represents 8-oxo-dG or 8-oxo-dA) at a molar ratio of 1: 1.2. Similarly, primer DNA (5′-CTTCCCTAGGAATT-3′) labeled with Cy3 at the 5′-end was annealed with template DNA (5′-GCGCG CTTCTGGCCAATTGCAGAATTCCTAGGGAAG-3′, where TT represents a *cis-syn* thymine dimer) at a ratio of 1 : 1.2. The template/primer containing 8-oxo-dG or 8-oxo-dA were incubated with 5 nM of Polη and R61K, or 10 nM of wild-type Polκ and 100 nM of Y112A. The reaction buffer contained 5 μM of unaltered dNTPs, and the reactions were incubated for 10 min at 37°C. The template/primer that contained the thymine dimer was incubated with 1, 5 and 20 nM of either wild-type Polη or R61K in the reaction buffer. This reaction buffer contained 250 μM dNTPs, and the reactions were incubated for 5 min at 37°C. The products were analyzed as described earlier.

### Modeling 8-oxo-dGTP in the active site of Polη

Models were created of 8-oxo-dGTP in the *syn* conformation opposite a dA residue and in the *anti* conformation opposite a dC residue in the active site of yeast Polη by 2007.09 version of the Molecular Operating Environment (MOE: Chemical Computing Group Inc., Montreal, Canada). These models were based on the reported crystallographic structures [PDB#: 2R8J (21)]. The active site of yeast Polη was displayed with Gaussian surfaces. The template and primer sequences were 3′-CACCTACT CX-5′ and 5′-GTGGATGAG-3′, respectively, where X represents the dA or dC that was paired with 8-oxo-dGTP.

## RESULTS

### The steric gate of Polκ is involved in the orientation of incoming 8-oxo-dGTP

The steric gate amino acids, which distinguish between dNTP and rNTP, are highly conserved. In most Pols, including those in the Y-family, phenylalanine or tyrosine forms the steric gate (29). In human Polκ, Y112 acts as the steric gate and also plays important roles in both the insertion of dCTP opposite a benzo[a]pyrene diolepoxide-$N^2$-dG adduct in the template DNA and the extension of mismatched termini (31). In Polη, F18 is assumed to be the steric gate, based on the amino acid sequence alignment and the crystallographic structure comparison with yeast Polη (Supplementary Figure S1) (30,33,34). We found that the mutant of Polη with the alanine substitution of F18 (F18A) was able to incorporate both rNTPs and dNTPs into DNA. However, its ability to incorporate dNTPs was substantially attenuated compared to the native Pol (data not shown). As the steric gates lie adjacent to the incoming dNTPs, they may affect the specificity incorporating oxidized dNTPs into DNA. To examine the possibility, we compared the specificities of Polκ versus Y112A and Polη versus F18A for preferentially pairing 8-oxo-dGTP with template dA. We found that Polκ showed a preference for pairing 8-oxo-dGTP with template dA (Figure 1A). However, this preferential pairing was absent in Y112A, which

paired 8-oxo-dGTP with both dA and dC with nearly equal frequency. The kinetic analyses indicated that the substitution of Y112 with alanine reduced the efficiency ($k_{cat}/K_m$) of pairing 8-oxo-dGTP with template dA by more than 200-fold. This resulted in nearly equal frequencies of pairing 8-oxo-dGTP with template dA and dC (Table 1). In contrast, both the wild-type Polκ and the Y112A mutant showed similar specificities for mainly incorporating 8-oxo-dATP opposite dT and 2-OH-dATP with dT and dG (Figure 1B and C).

We also examined the specificity of wild-type Polκ and Y112A for translesion DNA synthesis across 8-oxo-dG and 8-oxo-dA lesions in template strands. We found that both Pols had similar specificity for inserting dATP and, less frequently dCTP, opposite a template 8-oxo-dG; both also preferentially inserted dTTP opposite to a template 8-oxo-dA (Supplementary Figure S2). These

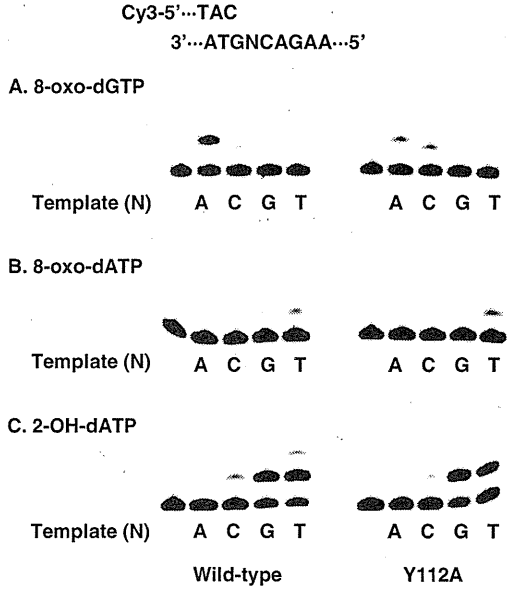


**Figure 1.** Incorporation of oxidized dNTPs into DNA by Polκ and its Y112A mutant. The primer/template DNA (100 nM, N in the template strand represents A, C, G or T) was incubated with wild-type Polκ (10 nM) or Y112A mutant (100 nM) in the presence of 50 μM 8-oxo-dGTP (**A**), 8-oxo-dATP (**B**) or 2-OH-dATP (**C**) for 10 min at 37°C. Extended primers were separated by denaturing PAGE. The first lanes represent the results of control experiments where no dNTPs were added to the reaction mixtures.

data indicated that the Y112 residue in Polκ was involved in the orientation of incoming 8-oxo-dGTP opposite dA, but not other specificity, i.e. incorporating 8-oxo-dATP or 2-OH-dATP into DNA or for a translesion bypass across an oxidized dG or dA in template strands.

In Polη, the corresponding substitution of F18 by alanine did not alter the specificity for incorporating oxidized dNTPs, including 8-oxo-dGTP, into DNA (Supplementary Figure S3). Therefore, we concluded that the steric gate of Polκ, but not Polη, was critical for inducing incoming 8-oxo-dGTP into the *syn* conformation in the active site, thereby facilitating its pairing with dA.

### R61 of Polη determines specificity for pairing 8-oxo-dGTP with template dA

As F18 did not appear to be involved in the orientation of 8-oxo-dGTP in the active site of Polη, we investigated other amino acids that might influence its specificity for incorporating 8-oxo-dGTP into DNA. We reasoned that R61 was the best candidate, because it was predicted to lie adjacent to the base of the incoming dNTP. Thus, we substituted R61 with alanine, methionine, asparagine, glutamine, histidine or lysine. We also changed I48 to alanine, serine, methionine, phenylalanine, asparagine, glutamine, aspartic acid or glutamic acid because it was also predicted to lie close to the base of the incoming dNTP. We found that R61A, R61M, R61N, R61Q, R61H and all the I48 mutants displayed similar specificity to the wild-type Polη and/or exhibited extremely low abilities to incorporate 8-oxo-dGTP into DNA (Supplementary Figure S4). However, we found that R61K was able to pair 8-oxo-dGTP with dC or dA with nearly equal specificity (Figure 2A). In contrast, the wild-type Polη preferentially paired 8-oxo-dGTP with dA (Figure 2A). In addition to changing the preference for incorrect pairing of 8-oxo-dGTP, R61K paired 8-oxo-dATP more efficiently with dT than with dG. In contrast, the wild-type Polη showed almost equal specificity for pairing 8-oxo-dATP with dT and dG (Figure 2B). However, R61K exhibited equal specificity for pairing 2-OH-dATP with dG, dT and dC, and less efficiency for pairing with dA; this specificity was similar to that observed for the wild-type Polη (Figure 2C). The wild-type Polη and R61K showed similar translesion activities for DNA synthesis across 8-oxo-dG, 8-oxo-dA, or a thymine dimer in the template strands

**Table 1.** Steady-state kinetic parameters for 8-oxo-dGTP by wild-type Polκ and Y112A mutant

| Template/dNTP | $k_{cat}$, $min^{-1}$ | | $K_m$, μM | | $k_{cat}/K_m$, $\mu M^{-1}$ $min^{-1}$ | | Y112A/WT |
|---|---|---|---|---|---|---|---|
| | WT[a] | Y112A | WT | Y112A | WT | Y112A | |
| dA/dTTP | 14 ± 3.0 | 9.2 ± 3.5 | 4.3 ± 2.0 | 72 ± 52 | 3.3 | 0.13 | 1/26 |
| dA/8-oxo-dGTP | 2.1 ± 0.38 | 0.029 ± 0.0052 | 83 ± 34 | 300 ± 140 | 0.026 | 0.000096 | 1/270 |
| dC/dGTP | 4.4 ± 0.64 | 5.4 ± 0.33 | 2.1 ± 0.84 | 20 ± 3.4 | 2.1 | 0.28 | 1/7.7 |
| dC/8-oxo-dGTP | 0.70 ± 0.12 | 0.11 ± 0.030 | 290 ± 120 | 660 ± 360 | 0.0024 | 0.00016 | 1/15 |

[a]WT: wild-type Polκ

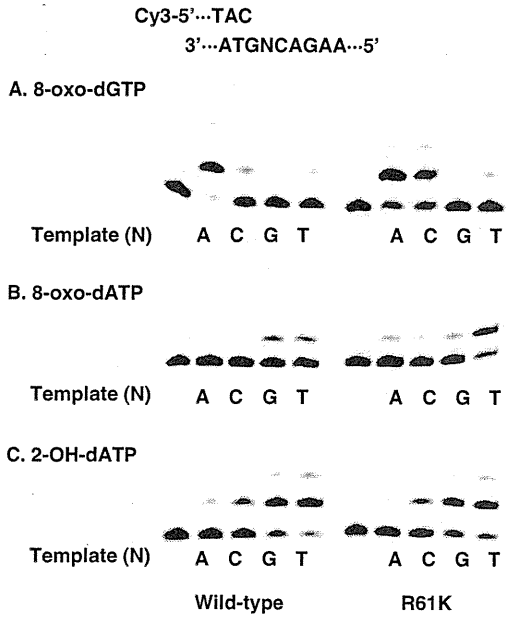


**Figure 2.** Incorporation of oxidized dNTPs into DNA by Polη and its R61K mutant. The primer/template DNA (100 nM, N in the template strand represents A, C, G or T) was incubated with wild-type Polη and R61K mutant (5 nM) in the presence of 50 μM 8-oxo-dGTP (**A**), 8-oxo-dATP (**B**) or 2-OH-dATP (**C**) for 10 min at 37°C. Extended primers were separated by denaturing PAGE. The first lanes represent the results of control experiments where no dNTPs were added to the reaction mixtures.

(Supplementary Figure S5). Thus, the effect of the R61K mutation appeared to be specific for conferring specificity for the incorporation of 8-oxo-dGTP and 8-oxo-dATP into DNA.

To quantitatively compare the efficiencies ($k_{cat}/K_m$) of incorporating 8-oxo-dGTP and 8-oxo-dATP into DNA among the wild-type Polη, R61K and R61A, we determined the kinetic parameters of each Pol for incorporating unaltered and oxidized dNTPs into DNA (Table 2). We found that the kinetic parameters for pairing unaltered dNTPs with the correct template bases were almost identical between the wild-type Polη and R61K. Likewise, the kinetics were not substantially different between the two Pols for pairing 8-oxo-dGTP and 8-oxo-dATP with incorrect template bases (8-oxo-dGTP with dA and 8-oxo-dATP with dG). However, R61K exhibited efficiencies that were 24-fold and 14-fold higher than wild type for correctly pairing 8-oxo-dGTP with dC and pairing 8-oxo-dATP with dT. Similarly, R61A exhibited efficiencies that were 1.7-fold higher than wild type for pairing both 8-oxo-dGTP and 8-oxo-dATP with dC and dT, respectively. These results suggested that R61 in Polη specifically inhibited pairing the C8-oxidized deoxypurine triphosphates with the correct template bases; i.e. 8-oxo-dGTP with dC and 8-oxo-dATP with dT. We concluded, therefore, that R61 was critical for orienting the incoming 8-oxo-dGTP into the *syn* conformation in the active site of Polη.

## DISCUSSION

Oxidation of the nucleotide pool can be a source of DNA damage when oxidized dNTPs are incorporated into DNA by Pols during chromosome replication (35). However, oxidized dNTPs are generally poor substrates for Pols. For example, calf thymus Polδ incorporated 8-oxo-dGTP into DNA with only about $10^{-4}$ times the efficiency showed for incorporating unaltered dGTP; moreover, the Pol exhibited a preference for correctly pairing 8-oxo-dGTP with template dC (36). Several other Pols exhibited poor efficiencies for 8-oxo-dGTP incorporation into DNA, including human Polγ, T7 Pol exo$^-$, HIV reverse transcriptase, *E. coli* Pol II, ϕ29 Pol and Klenow exo$^-$ (37,38). An exception may be human Polβ, which incorporated 8-oxo-dGTP into DNA with 10–20% of the efficiency it showed for unaltered dGTP incorporation, and it showed a preference for incorrect pairing with template dA (39). Calf thymus Polα incorporated 2-OH-dATP with <1% and 0.1% of the efficiencies it showed for incorporating unaltered dATP and dGTP, respectively; moreover, the Pol showed a similar preference for pairing 2-OH-dATP with template T and C (40). In this respect, it is interesting that Y-family Pols from bacteria, Archaea and humans exhibit a preference for incorrectly pairing 8-oxo-dGTP with template dA (21,22,24) and human Polη incorporates it with a relatively high efficiency (23,41).

To examine the mechanisms underlying the conserved specificity of Y-family Pols for incorrectly pairing 8-oxo-dGTP with template dA, we substituted amino acids of human Polη and Polκ, which might modulate the specificity. The results indicated that R61 of Polη and Y112 of Polκ played important roles in the preferential pairing of 8-oxo-dGTP with template dA. In Polη, when R61 was substituted with alanine, the ratio of pairing of dA to 8-oxo-dGTP compared to pairing of dC was reduced from 660:1 in wild type to 65:1 in R61A (0.79:0.0012 in wild type and 0.13:0.0020 in R61A, Table 2). Moreover, the substitution of R61 with lysine (R61K) resulted in the ratio of pairing of dA to 8-oxo-dGTP compared to pairing of dC of 7:1 (0.19:0.028 in R61K, Table 2, Figure 2). In Polκ, the Y112A mutant had less preference for incorrectly pairing 8-oxo-dGTP with template dA (Figure 1). This was primarily because the replacement of Y112 with A more severely reduced its efficiency for pairing 8-oxo-dGTP with template dA (270-fold reduction) compared to the reduction in its efficiency for pairing with template dC (15-fold reduction) (Table 1). Thus, the ratio of pairing of dA to 8-oxo-dGTP compared to pairing of dC was reduced from 11:1 to 0.6:1 by the Y112A amino acid substitution (0.026:0.0024 in wild type and 0.000096:0.00016 in Y112A, Table 1). In addition to its role as the steric gate, Y112 was previously shown to be involved in bypass DNA synthesis; e.g. pairing dCTP with template a benzo[a]pyrene diol epoxide-$N^2$-dG adduct and the extension of primers with terminal mismatches (31). Thus, the amino acid at the 112 position may interact with both the base and the sugar moiety of the incoming dNTPs. These data suggest that

**Table 2.** Steady-state kinetic parameters for C8-oxidized dNTP by wild-type Polη and R61 mutants

| Template/dNTP | hPolη | $k_{cat}$, $min^{-1}$ | $K_m$, $\mu M^{-1}$ | $k_{cat}/K_m$, $\mu M^{-1}$ $min^{-1}$ | Related efficiency |
|---|---|---|---|---|---|
| dA/dTTP | | | | | |
| | WT[a] | 28 ± 2.7 | 5.1 ± 1.4 | 5.4 | 1.0 |
| | R61K | 40 ± 5.9 | 17 ± 4.5 | 2.3 | 0.43 |
| | R61A | 8.0 ± 1.2 | 12 ± 3.5 | 0.7 | 0.13 |
| dA/8-oxo-dGTP | | | | | |
| | WT | 18 ± 1.8 | 22 ± 6.2 | 0.79 | 1.0 |
| | R61K | 21 ± 4.8 | 110 ± 41 | 0.19 | 0.24 |
| | R61A | 5.4 ± 1.3 | 42 ± 23 | 0.13 | 0.16 |
| dC/dGTP | | | | | |
| | WT | 11 ± 1.8 | 3.1 ± 1.2 | 3.6 | 1.0 |
| | R61K | 17 ± 1.2 | 4.6 ± 0.71 | 3.7 | 1.0 |
| | R61A | 6.3 ± 1.8 | 6.3 ± 3.5 | 1.0 | 0.27 |
| dC/8-oxo-dGTP | | | | | |
| | WT | 0.87 ± 0.21 | 720 ± 320 | 0.0012 | 1.0 |
| | R61K | 4.6 ± 0.58 | 160 ± 49 | 0.028 | 23 |
| | R61A | 0.37 ± 0.050 | 180 ± 56 | 0.0020 | 1.7 |
| dG/dCTP | | | | | |
| | WT | 33 ± 2.9 | 3.2 ± 87 | 10 | 1.0 |
| | R61K | 38 ± 3.3 | 7.4 ± 1.5 | 5.1 | 0.49 |
| | R61A | 14 ± 2.1 | 3.7 ± 1.7 | 3.7 | 0.35 |
| dG/8-oxo-dATP | | | | | |
| | WT | 0.90 ± 0.16 | 370 ± 150 | 0.0024 | 1.0 |
| | R61K | 0.78 ± 0.14 | 510 ± 190 | 0.0015 | 0.63 |
| | R61A | 0.33 ± 0.063 | 180 ± 100 | 0.0018 | 0.74 |
| dT/dATP | | | | | |
| | WT | 18 ± 2.4 | 5.7 ± 1.5 | 3.1 | 1.0 |
| | R61K | 22 ± 2.8 | 6.8 ± 1.7 | 3.2 | 1.0 |
| | R61A | 14 ± 4.6 | 11 ± 5.7 | 1.3 | 0.43 |
| dT/8-oxo-dATP | | | | | |
| | WT | 0.56 ± 0.070 | 150 ± 46 | 0.0036 | 1.0 |
| | R61K | 3.2 ± 0.33 | 61 ± 16 | 0.052 | 14 |
| | R61A | 0.26 ± 0.016 | 43 ± 9.2 | 0.0061 | 1.7 |

[a]WT: wild-type hPolη

Y112 may stabilize the pairing of 8-oxo-dGTP with template dA in the active site of the Pol. In contrast, the F18 position of Polη, which corresponds to Y112 in Polκ, did not appear to play a role in the specificity for pairing 8-oxo-dGTP with template dA. Therefore, amino acids involved in the specificity of incorporating 8-oxo-dGTP into DNA are not conserved between Polη and Polκ, despite the fact that they belong to the same Y-family.

In Polη, the substitution of R61 with lysine elevated its preferences for pairing 8-oxo-dGTP with dC and 8-oxo-dATP with dT without affecting other activities; e.g. incorporating unaltered dNTP into DNA or bypassing oxidized dG or dA or thymine dimers in template DNA (Figure 2, Table 2, Supplementary Figure S5). These results suggested that R61 specifically inhibited the ability to correctly pair C8-oxidized dNTPs with template DNA. To investigate how R61 modulated the conformation of incoming 8-oxo-dGTP in the active site, we modeled the predicted *syn* and *anti* structures of 8-oxo-dGTP paired with dA or dC in the active site of yeast Polη. In this model, arginine 73, which corresponds to R61 of human Polη, was substituted with lysine or alanine (Figure 3). The model suggested that the side chain of arginine may constitute a steric constraint, because it would not accommodate the $O^8$ of an 8-oxo-dGTP in the *anti* conformation, but could accommodate it in the *syn* conformation (Figure 3A). This may be the basis for the preference shown by Polη for pairing 8-oxo-dGTP with template dA. Interestingly, when the arginine was substituted with lysine, the model indicated that the ε-amino group and $O^8$ of 8-oxo-dGTP in the *anti* conformation may be interacted electrostatically (Figure 3B). These results suggested that the lysine, but not arginine, might stabilize 8-oxo-dGTP in the *anti* formation; this would enhance the preference for correctly pairing 8-oxo-dGTP with template dC. In the case of alanine, the side chain did not interact with 8-oxo-dGTP (Figure 3C). Thus, the slight enhancement in the preference of R61A for pairing 8-oxo-dGTP with template dA may be due to the lack of a steric constraint of R61 in the active site of Polη. This prediction, based on model structure, could also be applicable to the preference of Polη for correctly pairing 8-oxo-dATP with template dT; the arginine may not accommodate the 8-oxo-dATP in the *anti* conformation, and the substituted lysine may induce 8-oxo-dATP to assume the *anti* conformation with the electrostatic interaction, and thus, would result in pairing with template dT. These predictions are in accordance with our biochemical findings that R61A and R61K exhibited increased preferences for pairing 8-oxo-dGTP with dC and 8-oxo-dATP with dT compared to the wild-type Polη (Table 2). Therefore, R61 appeared to play a critical role in modulating the *anti* or *syn* conformation of 8-oxo-dGTP in the active site of Polη. In human

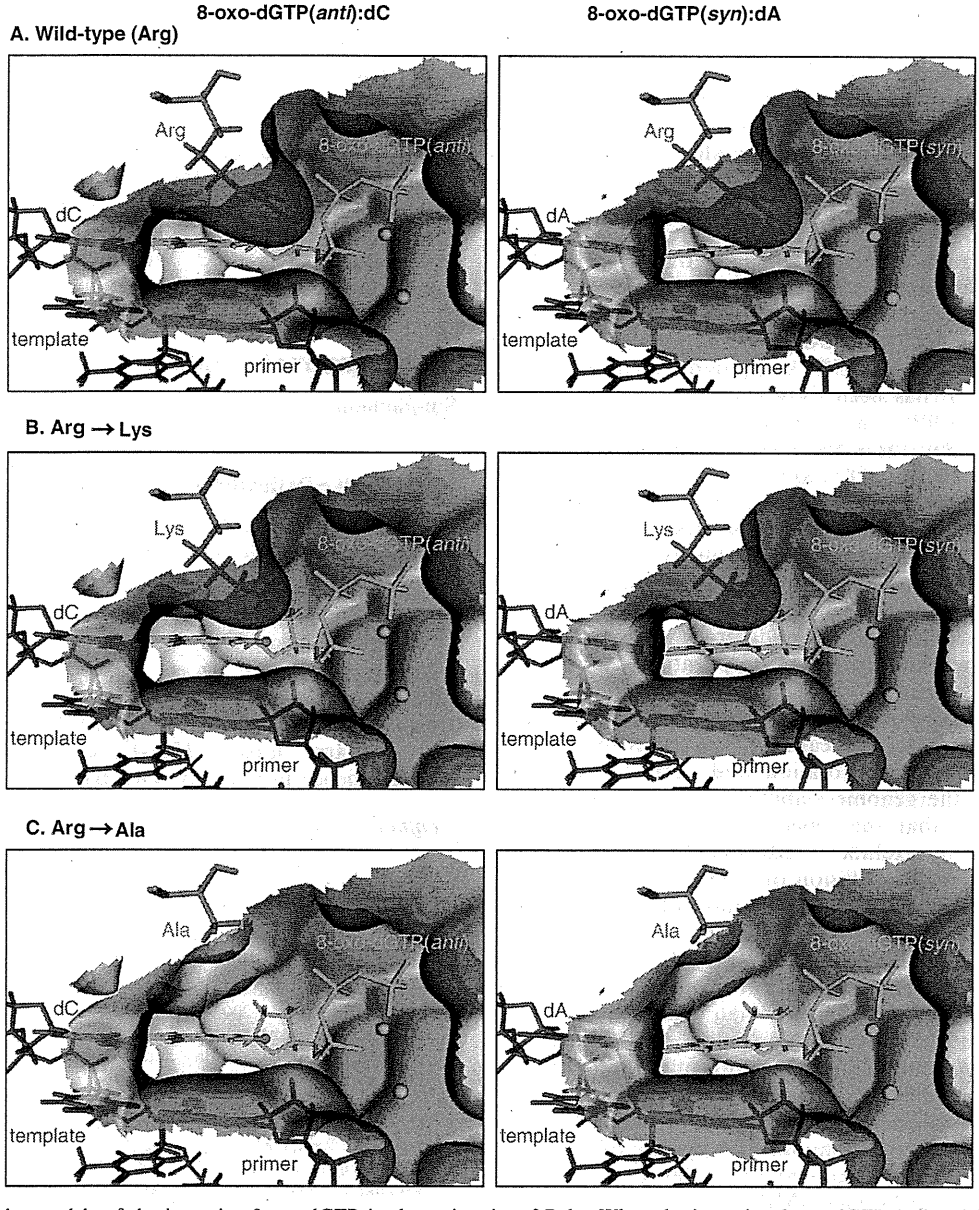


**Figure 3.** Molecular models of the incoming 8-oxo-dGTP in the active site of Polη. When the incoming 8-oxo-dGTP (cyan stick) forms the *anti* conformation (left panels), the side chain of arginine (displayed as a purple stick) may sterically clash with $O^8$ (red ball) of the incoming 8-oxo-dGTP, which may be the reason for the poor incorporation of 8-oxo-dGTP opposite template dC (green stick) (**A**). Proper pairing with template dC can be achieved, however, when arginine is substituted with lysine (**B**) or alanine (**C**) because of no steric hindrance. An electrostatic interaction between the lysine residue and $O^8$ of 8-oxo-dGTP may facilitate the incorporation of 8-oxo-dGTP opposite template dC (B). When the incoming 8-oxo-dGTP forms the *syn* conformation (right panels), there appear no steric or electrostatic interactions between the amino acids and $O^8$ of 8-oxo-dGTP (A–C). All models were constructed based on the crystal structure of yeast Polη [PDB#2R8J (21)]. The active site of Polη is displayed as Gaussian surface (colored according to its electric charge).

Polι, there is a lysine residue at the position corresponding to the R61 of Polη (Supplementary Figure S1). However, Polι always paired 8-oxo-dGTP with dA. Thus, the mechanism underlying the preference of Polη for pairing 8-oxo-dGTP with template dA may be unique to this enzyme.

Human Polβ has an asparagine in its active site, i.e. N279, that was shown to be involved in its specificity for the incorporation of oxidized dNTPs (39). Polβ was shown to preferentially pair 8-oxo-dGTP with template dA. The substitution of N279 with alanine (N279A) reduced the activity of Polβ incorporating 8-oxo-dGTP with template dA by almost 1000-fold, but it decreased the activity incorporating it with template dC by about 3-fold. Thus, the ratio of pairing of dA to 8-oxo-dGTP compared to pairing of dC was altered from 24 : 1